International Journal of Engineering Science 207 (2025) 104174

Contents lists available at ScienceDirect

International Journal of Engineering Science

journal homepage: www.elsevier.com/locate/ijengsci

Full Length Article

On nonlinear 3D electro-elastic numerical modeling of two-phase inhomogeneous FG piezocomposites reinforced with GNPs

Mohammad Malikan [a,b,*], Shahriar Dastjerdi [c], Magdalena Rucka [a], Mehran Kadkhodayan [c]

[a] Department of Mechanics of Materials and Structures, Faculty of Civil and Environmental Engineering, Gdańsk University of Technology, ul. Gabriela Narutowicza 11/12, 80-233 Gdańsk, Poland
[b] Department of Plastics Engineering, University of Massachusetts Lowell, 1 University Ave, Lowell, Massachusetts 01854, USA
[c] Department of Mechanical Engineering, Ferdowsi University of Mashhad, Mashhad 91775-1111, Iran

ARTICLE INFO

Keywords:
Numerical model
Nonlinear 3D elasticity
Piezoelectricity
FGMs
Graphene nanoplatelets

ABSTRACT

The novelty here comes from not only the perfect nonlinear three-dimensional (3D) electro-elasticity investigation but also the mixed material itself. The literature widely showed mechanical assessments on the piezoelectric structures; however, a lack of nonlinear three-dimensional elasticity studies has been witnessed on these kinds of smart materials. Therefore, a nonlinear 3D elasticity-piezoelectricity coupling is considered in this study. What is more, this research brings about an era in the field of sensing manufacturing such as sensors and actuators by proposing the construction of these devices in an advanced composite framework. The piezoelectric medium can be electro-mechanically improved with the aggregation of graphene platelets/nanoplatelets (GPLs/GNPs) based on the functionally graded (FG) composition. The assumption for such a smart composite has been made to provide higher flexibility smart tools while their elastic strength can also get further. To accomplish this, the derivation of a rigorous mathematical model has come out for a transversely isotropic inhomogeneous FG-piezoelectric beam-like sensor/actuator using 3D kinematic displacements, geometrically nonlinear strains, Lagrange technique, 3D stress-strains tensors, linear elastic material, and in particular Halpin-Tsai micro-mechanic model. Numerical modeling has been built by the generalized differential quadrature (GDQ) technique. A comprehensive parametric study has also been established for intelligent FG beams.

1. Introduction

The term “piezoelectric” means electricity that is caused by pressure. This word is derived from two Greek words; “piezo” which means ‘to press’, and “electron”. In fact, piezoelectric structures are materials that, when pressure or tension is applied to them, an electric charge appears on their certain levels. This phenomenon is called the “Direct Piezoelectric Effect”, which is a reversible process. That is, conversely, when a material with this property is placed in an electric field, its dimensions will change (Reverse Piezoelectric Effect). If it is inverted to apply tension or pressure, the direction of polarization of electric charges is also reversed (Arnau and Soares, 2009; Cady, 1964; Curie and Curie, 1880).

* Corresponding author.
E-mail addresses: mohammad.malikan@pg.edu.pl, malikan.mohammad@gmail.com, mohammad.malikan@yahoo.com (M. Malikan).

https://doi.org/10.1016/j.ijengsci.2024.104174
Received 18 September 2024; Received in revised form 27 October 2024; Accepted 27 October 2024
Available online 27 November 2024

Nomenclature

a_{gnp}	Average length of GNPs
h_{gnp}	Average thickness of GNPs
b_{gnp}	Average width of GNPs
u and w	Axial and lateral displacements
V	Domain's volume
$\aleph$	Displacement vectors
u_i $(i = 1,3)$	Displacement in the x- and z- directions
ε_{ij}	Elastic strains
σ_{ij}	Elastic stresses
D_j	Electric displacements
d_i	Electric fields
Φ	Electric potential function
ϕ	Electric potential's magnitude in the mid-plane
V_0	External electric voltage
F	External mass loads
C_{ijkl}	4th-order pure elasticity tensor
$\Re$	Free energy density
h	Initial thickness of the beam
L	Initial effective length of the beam
b	Initial width of the beam
N^0_{xx}	In-plane electric force
N_L	Number of layers in FGMs
ν_{ij}	Poisson's ratio
κ_{ij}	2nd-order dielectric tensor
e_{ijk}	3rd-order piezoelectric tensor
G_{ij}	Shear elastic modulus
U	Strain energy
z	Thickness coordinate
ψ	3D electric potential's magnitude
∇	3D nabla operator
q	Transverse static load
$V^{(k)}_{gnp}$	Volume fractions of GNPs in each layer
g^*_{gnp}	Volume fractions of GNPs in medium
W	Work done by external forces
E_i	Young's modulus

All piezoelectric structures are generally non-conductive and can be divided into two groups: crystals and ceramics. Barium titanate, Lead zirconate titanate (PZT), and lithium niobate can be examples of piezoelectric structures. These synthetic materials have a more impressive effect than quartz (the first known piezoelectric material) and other natural piezoelectric substances. Compared to quartz (Wudy et al., 2009), PZT produces a greater potential difference for the same amount of applied mechanical stress. Also, applying an electric potential difference to PZT provides more mobility (ABC 2021). Lead zirconate titanate was produced in 1952 by the Tokyo Institute of Technology (Tanaka, 1982). This material is made and produced from two chemical elements; lead and zirconium, and a chemical compound called titanate at high temperatures. PZT is usually used to make ultrasonic transducers, data storage, structural health monitoring, ceramic capacitors, sensors and actuators, sonars, piezoelectric patches, naval hydrophones, acoustic applications, and resonators in electronic equipment (Bell and Deubzer, 2018; Chróścielewski et al., 2019; Fan et al., 2022; He et al., 2024; Karami and Shahsavari, 2019; Kędra and Rucka, 2017; Manbachi and Cobbold, 2011; Markov et al., 2023; Moreno-Mateos et al., 2024; Partovi Shabestari et al., 2019; Silva et al., 2023; Singh et al., 2022).

A piezoelectric sensor can produce an output signal when it experiences strain without needing an external source or voltage and vice versa for a piezoelectric actuator. This makes them a popular choice in many applications. The use of these sensors/actuators in several industries is growing remarkably. The piezoelectric sensor does not require any power to continuously monitor an environment. This type of sensor is the most sensitive pressure gauge technology that provides accurate, stable, and repeatable electrical output (Du et al., 2024; Gautschi, 2002; Steinem and Janshoff, 2005).

Heretofore, researchers know that ceramic materials possess a fatal flaw concerning their inherent brittleness (Aoki et al., 2024; Deforming brittle, 2023). The inherent characteristics of ceramic structures including chemical bonds and microstructures affect the brittleness. Notably, such frangibility influences the efficiency of workability of piezoelectric ceramics. Many scientists are working to propose effectual solutions to overcome the brittleness of these structures. To confront this challenge, it requires to focus on the

chemical aspects (Yamada et al., 1998). Nevertheless, on the contrary, this task can be accomplished by utilizing composite sciences.

In engineering up-to-date science, functionally graded materials (FGMs) are those with advanced heterogeneous structures. Such materials possess excellent properties not only mechanical but electrical and thermal as well, making FGMs to be widely used. In the group of FGM structures, all material properties vary continuously from one point to another depending on a predefined law. The variation is caused by a gradual change in the volume ratio of the constituent materials (Argatov and Sabina, 2022; Dastjerdi and Akgöz, 2018; Dastjerdi et al., 2022; Dastjerdi et al., 2021,; Dastjerdi et al., 2023,; Golmakani et al., 2023; Jena et al., 2021; Kaplunov et al., 2022; Karami and Ghayesh, 2023; Malikan and Eremeyev, 2020; Malikan et al., 2022; Shahriar Dastjerdi et al., 2023; Vaccaro, 2022).

Of the strengths of FGMs compared to laminated composites, one can say that these materials have high resistance to mechanical loads, high-temperature capacity, less crack prospect, and less possibility of separating the layers (delamination). In light of the competencies of the FGMs, numerous scientists and engineers have manufactured various kinds of materials in the guise of FGMs (Saleh et al., 2020; Takagi et al., 2003). Takagi et al. (2003) fabricated a piezoelectric composite based on the PZT matrix and Platinum reinforcer in the form of FGMs via a sintering process. The FGM actuator has been evaluated mechanically and electrically. It was found that the mechanical properties of the piezocomposite will improve if Pt material is added to the PZT matrix. As a result, dielectric constant values become larger specifically with an increase in Pt powder, while the amounts of piezoelectric constants get smaller uniformly. However, the FGM actuator is not poor in the property of electrical induction compared to the PZT ceramic (PZTC) actuator. It can be concluded that the idea of producing sensors and actuators by FGMs is worth choosing.

Piezoelectric structures can be synthesized with several materials which normally lead to novel smart composites, named piezo-composites. This combination provides fundamental merits over standard piezoceramic structures. Many researchers and scientists have already shown the excellence of the concept of functionally graded composition while applying it to various materials (Saleh et al., 2020; Takagi et al., 2003). Upon dynamic as well as static conditions, the literature demonstrated that by such the composition, the superiorities could be the increase of the bonding strength (and fatigue-life), maximization of output displacement, enhancement of the stress redistribution, and decrease in the elastic stress (Samadhiya and Mukherjee, 2006; Taya et al., 2003; Wang and Noda, 2001). Moreover, having a higher flexible piezoelectric ceramic with consistent dielectric and piezoelectric features is a serious need for high-tech industries. In terms of energy harvesting, the further flexible piezoelectric sensor results in a more efficient energy harvester if the piezoceramic possesses a good electric permeability. Accordingly, the smart composite that will be assumed under this work can be a higher efficient sensor, actuator, transducer, energy harvester, etc., and the structure could be of interest to high-tech markets.

Thus, this research has given particular attention to proposing a piezocomposite by dint of the concept of functionally graded materials (FGMs). To fulfill this job, we replace the common piezoelectric structure with an FG-piezoelectric matrix. Consequently, this issue results in the alteration of all material constants (piezoelectric, elastic, and dielectric) through a determined dimension. At last, a computational model will be derived to perform this piece of research.

At this point, let us trace back to explore the research done close to this title. The background can be divided into two sections; first, three-dimensional analyzes can be surveyed in detail. Then, two-dimensional studies will be reviewed. It must be emphasized that due to the vast literature, we are not going to look into the small-scale sensors and actuators and the published works on the macro intelligent composite sensing elements will be expressed only. In terms of 3D studies of piezoelectric composite beam/plate/shell-like structures, Chen et al. (2004) examined 3D linear natural frequencies of FG piezoelectric hollow cylinders. Meanwhile, a compressible fluid flow has also filled the cylinder. The material constants of two piezoelectric materials, namely PZT4 and $Ba_2NaNb_5O_{15}$, have been taken into analysis by grading along thickness based on the two arbitrary functions. Zhong and Shang (2003) studied FG-piezoelectric laminates using exact linear 3D simply-supported boundary conditions. However, no specified reinforcer was considered and the material properties of the PZT4 laminated plate were supposed to vary exponentially in each layer along the thickness. Hosseini--Hashemi et al. (2010) used a 3D Ritz solution to extract linear natural frequencies for an annular/circular FG plate assembled with PZT4 layers. The study by Alibeigloo and Nouri (2010) inspected a static response of FG cylindrical shells with exponential distribution of material constants in the thickness direction which was integrated with non-FGM sensor and actuator layers. Akbari Alashti and Khorsand (2011) carried out linear thermo-elastic models of FG cylindrical shells integrating piezoelectric layers by the use of three-dimensional elasticity. Their model obviously did not consider a piezoelectric matrix and any micro reinforcers. They took the advantage of differential quadrature method (DQM) to provide numerical results. Li et al. (2011) evaluated the bending and tension behaviors of FG piezoelectric circular plates assuming material isotropy with the help of 3D analytical models. However, their equations indicate that they have used stress resultants in the thickness domain which cannot be true for a 3D model due to the fact that membrane forces can appear for 2D plane stress/strain problems only. And a factual 3D medium does experience thickness deformation. Javanbakht et al. (2012) by the ground of 3D elasticity, analysed linear dynamics of an FG piezoelectric panel using power-law distribution for all constants. Their FGM model was assumed to be made of ceramic and metal in a powder mixing. Jodaei et al. (2013) investigated the linear natural frequencies of an FG piezoelectric annular plate via a modified version of DQM. It was postulated that the material properties of PZT4 ceramic change through the thickness on the basis of an exponent-law variation. Kulikov and Plotnikova (2013) proposed a new approach by the use of the sampling surfaces method to implement a 3D exact model of FG piezo-laminated plates. The FGM has been developed by PZT4 and 5A and their material constants have been varied exponentially and linear governing equations have been given. Wang et al. (2016) derived 3D analytical models to study the linear bending of FGM annular piezocomposite plates vertically graded by an exponential variation. Liang et al. (2019) explored linear 3D dynamical characteristics of FG cylindrical piezo panels by introducing Durbin's inversion, space state approach, Laplace transform, and DQM in 3D spaces. The electro-elastic properties of PZT4 and PZT5H were changed by both power-law and exponential functions. Zenkour and Aljadani (2020) presented a linear quasi-3D model to investigate the stability of an FG piezocomposite plate with PZT4 and PZT5H

material that their properties vertically differ by the power-law mixture rule. Howbeit, the quasi-3D models and higher-order shear deformation theories can effectively predict large deflections and complicated models (Karami and Ghayesh, 2024; Karami et al., 2024), but they do not possess thickness deformations and can be a simplification for 3D domains only. They commonly provide information about mid-plane displacements. That means, in comparison with the fully 3D elasticity, 3D elasticity enables having information about deformations through the whole points of the domain except the mid-plane. What is more, 3D elasticity has no assumptions in the kinematic displacement field, which is typically inside the quasi-3D models. Xia and Gu (2021) attempted to obtain a linear 3D solution based on the finite difference method (FDM) for piezoelectric problems. No FGM assumption has been reported and simply a PZT4 material has been taken in hand. Singh et al. (2023) merged and connected FGM viscoelastic polymer layers with PZT5A ones to establish an FG-laminated rectangular plate and estimated time-dependent results. A merit of their work can be the representation and consideration of several viscoelastic models. Alshenawy et al. (2023) extended the 3D elasticity studies of FG piezoelectric shells employing strain gradient formulations. A nonlinear stability model has been calculated, though the stress resultants have also been involved. Two-dimensional elasticity studies can also be quoted here (Arefi et al., 2018; Ashoori and Sadough Vanini, 2017; Atai and Lak, 2016; Attar et al., 2021; Gerstner, 2010; Komijani et al., 2014; Le, 2017; Lin and Muliana, 2015,; Lu et al., 2021,; Rafiee et al., 2014; Shen and Yang, 2015; Wang and Xu, 2010; Yang et al., 2023; Yiqi and Yiming, 2010). Nonetheless, for the generality and not losing the main scope, the 2D literature is not embraced to be discussed.

Last but not least, FEM-based commercial codes are widely available for various mechanical analyzes, such as nonlinearity, complex geometries, etc. (Moghadasi et al., 2024). However, not to mention that a piezoelectric FGM cannot be precisely modelled

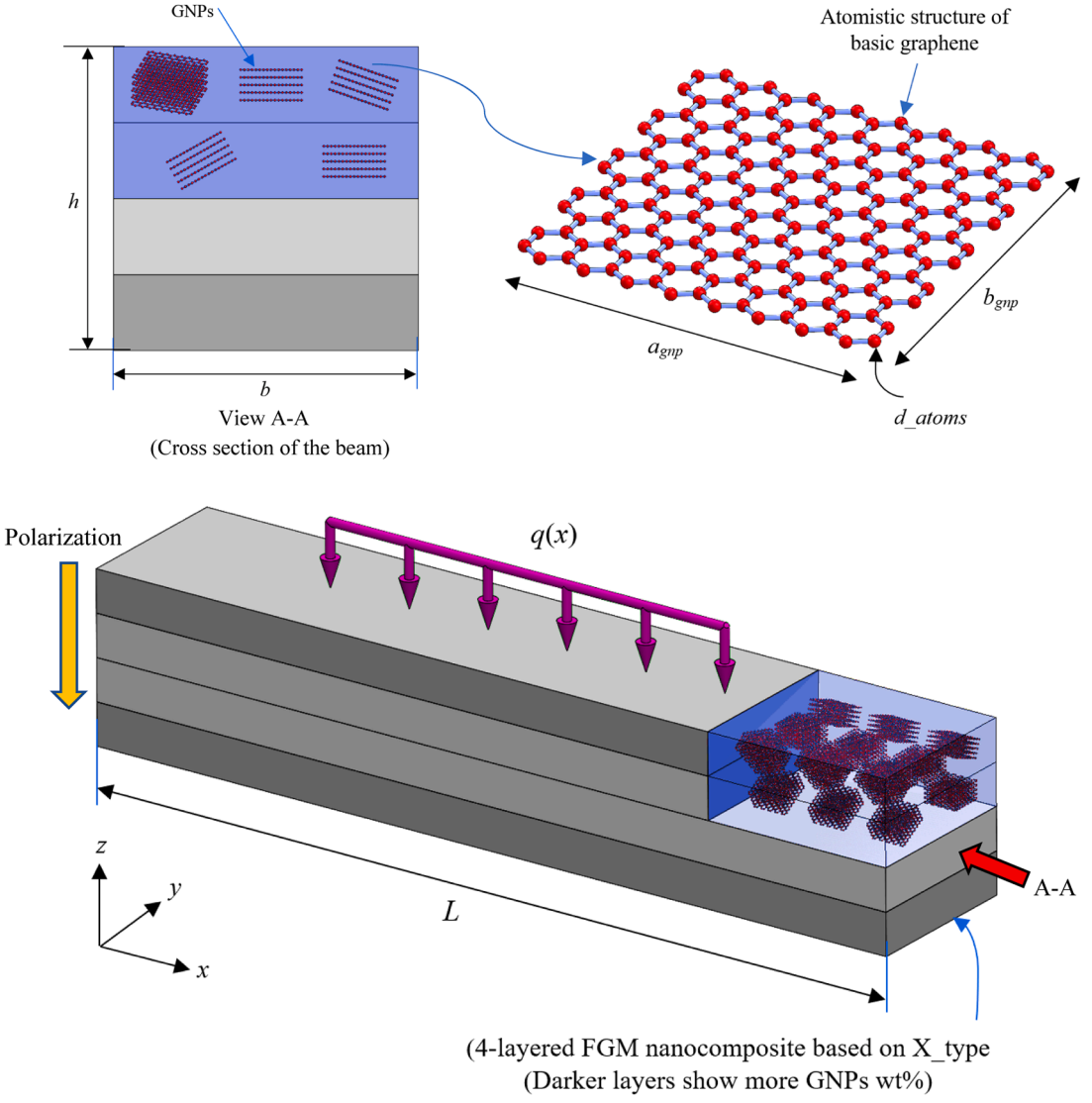

Fig. 1. The smart beam reinforced with GNPs based on random distributions (Scaling is not real; the pictures are original and have been designed in SolidWorks 2023).

with these tools and a mathematical model can handle such problems more methodically. The mathematical model can be an all-inclusive analysis in which a detailed model can be granted compared with the FEM-based software where the basic computer calculations behind the visualized model are unclear. FEM-based software is highly element-dependent, and the accuracy of the result is directly contingent on the mesh algorithm, kind of employed element, size of the element, etc., but mathematical models rely on the exact elasticity and analytical processes where everything can be controlled explicitly. Additionally, in contrast to commercial software, mathematical models meet a fast-doing operation . All in all, pertaining to intricate geometries, FEM-based software is preferred, but other side, in the matter of difficult physics, theoretical models can be a priority.

Based on what we have faced above, there are no research and study for when the PZT can play the role of matrix being enriched with GNPs/GPLs powder, and all the above studies have discussed a piezoelectric layer in interconnection with other materials or an exponential variation of PZT material properties in line with the thickness. In addition to these, no nonlinear 3D study has been seen and all the above-mentioned literature utilized linear 3D models or nonlinear utilizing membrane forces. Nonlinear 3D elasticity with thickness variation is a quite complicated problem that will be studied in the present paper.

The organization of the paper is with respect to some sections. The 1st section, as it has already been evident, collected and probed the linked research background to represent the objective of the current research. The 2nd section is adjusted to gather all the essential mathematical theories and expressions to bring us to the point where the constitutive bending equations can be provided. The 3rd section will give the set of vital operations for the numerical solution. The solving method will be validated through Section 4. In continuation, the numerical results are depicted in the 5th section. Ultimately, the 6th section shortly describes the paper and renders the significant results achieved by this research.

2. Mathematical modeling

Let us position the continuum specimen in the Cartesian coordinate system (x, y, z) where the volume occupies a space of [0, L] × [0, b] × [0, h] each in order for the effective length, width, and thickness of the beam-like samples pictured in Fig. 1.

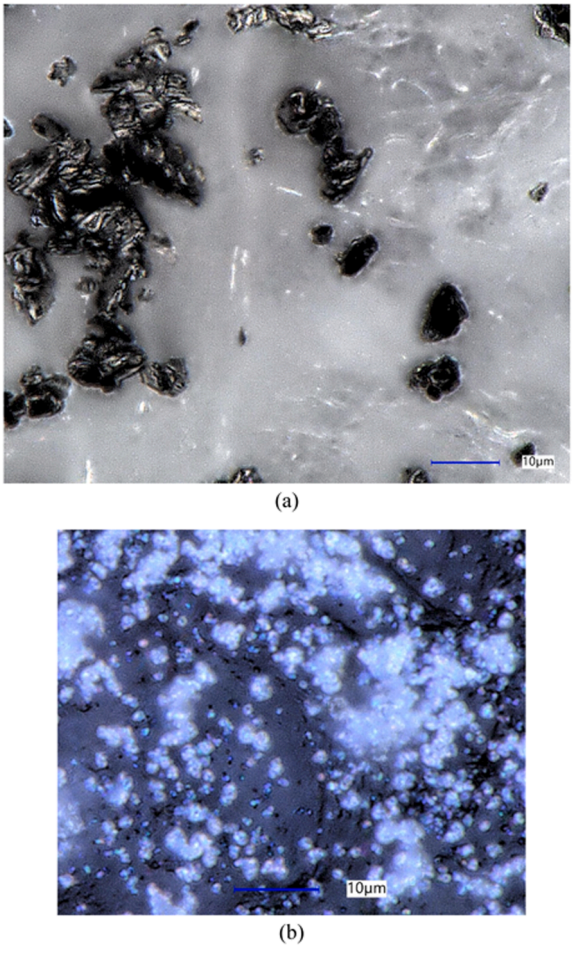

Fig. 2. Microscopic images for GNPs/GPLs (a) and PZT (b).

Graphene nanoplatelets/platelets (GNPs/GPLs) are termed as a kind of nanomaterial that comes from the basic graphene. Primary graphene comprises a monolayer carbon sheet that is the thinnest and strongest material ever discovered (Hassanzadeh-Aghdam, 2021; Yee and Ghayesh, 2023), although GNPs/GPLs incorporate multilayer graphene layers and encompass platelets-shaped carbon sheets (Fig. 2). Despite the outstanding properties of GNPs and their use in reinforcing polymeric nanocomposites, they have been negligibly used in smart matrices-based nanocomposites. Much research proved that GNPs have a better strengthening effect on the composites than carbon nanotubes (CNTs) due to the noticeable surface effect of GNPs that can play a key role in transferring the shear load between two phases of the nanocomposite. Moreover, GNPs are cheaper than CNTs in terms of production (Li et al., 2004). This fact persuades us that when it comes to nano-additives, GNPs can suggestively be utilized. By preparing Fig. 2, the microscopic images for GNPs and PZT can be seen that have been taken using Keyence VHX-7000 digital optical microscope at the Gdańsk University of Technology. The pictured materials belong to the next parts of the research grant on the experiments. Note that the used backgrounds are white and black sheets, respectively.

2.1. 3D elasticity-piezoelectricity

At this stage, a three-dimensional elasticity-piezoelectricity approach is adopted to possibly provide the electro-elastic coupling constitutive equations for the mechanics of the PZTC structure. The assumptions are diminished to isothermal conditions, and small deformations but large displacements. In order to state the first-order electric field (d) and the displacement vectors ($\aleph$), one writes

$$\aleph = \aleph(\alpha), \mathrm{d} = \mathrm{d}(\alpha) \tag{1}$$

where α stands as a position vector; $\aleph$is the displacement vector; and $d$shows electric fields.

It is the turn to demonstrate the electric enthalpy density ($\Re$) of piezoelectric elastic structures in the general quadratic representation as

$$\Re = \frac{1}{2}C_{ijkl}\varepsilon_{ij}\varepsilon_{kl} - e_{ijk}d_i\varepsilon_{ij} - \frac{1}{2}\kappa_{ij}d_id_j \tag{2}$$

where the introduced tensors are given by

C: 4th order elasticity tensor
ε: 2nd order strain tensor
e: 3rd order piezoelectric tensor
d: Electric field vector
κ: 2nd order dielectric tensor

The 3D constitutive equations for stress and electric displacement are shown below (Malikan and Eremeyev, 2020)

$$\sigma_{ij} = \Re_{,\varepsilon} = C_{ijkl}\varepsilon_{kl} - e_{kij}d_k \tag{3a}$$

$$D_j = -\Re_{,d} = e_{jkl}\varepsilon_{kl} + \kappa_{jk}d_k \tag{3b}$$

where σ_{ij} denotes elastic stresses; D_j displays the electric displacements.

It necessities to note that the thermal and pyroelectric effects have been crossed off from the analysis as the present problem does not intend to estimate heat. The tensors and vectors demonstrated by Eq. (3) are available as

$$\sigma = \begin{bmatrix} \sigma_{xx} & \sigma_{yy} & \sigma_{zz} & \tau_{yz} & \tau_{xz} & \tau_{xy} \end{bmatrix}^T \tag{4}$$

$$\varepsilon = \begin{bmatrix} \varepsilon_{xx} & \varepsilon_{yy} & \varepsilon_{zz} & \gamma_{yz} & \gamma_{xz} & \gamma_{xy} \end{bmatrix}^T \tag{5}$$

$$D = \begin{bmatrix} D_x & D_y & D_z \end{bmatrix}^T \tag{6}$$

$$d = -\begin{bmatrix} d_x & d_y & d_z \end{bmatrix}^T \tag{7}$$

Given the Hamilton's principle, the constitutive equations can be extracted (Malikan et al., 2023)

$$\delta\Big|_t\left(-\int_V UdV + W \right) = 0 \tag{8}$$

in which V is the domain's volume; U shows the strain energy; and W is the work done by external forces.

The following expression defines the work resulting from the external forces

$$\delta W = \int_V F \cdot \delta u + \int_{\partial V} t \cdot \delta u ds \tag{9}$$

where F is external mass loads; t is the time variable.

Keeping up the relations, a three-dimensional elasticity beam will be investigated by eliminating the y-axis changes. The 3D kinematic field of displacements can be expressed as (Malikan, 2024)

$$\begin{bmatrix} u_1(x,y,z) \\ u_3(x,y,z) \end{bmatrix} = \begin{bmatrix} u(x,z) \\ w(x,z) \end{bmatrix} \tag{10}$$

where u_i $(i = 1,3)$ are displacement in the x- and z- directions; u and w show axial and lateral displacements.

The usual geometrical approximations are discluded in the above kinematic displacements, which indicate the robustness of 3D elasticity analyzes.

The pure elastic strains can be easily obtained by manipulating with Lagrangian strains as (Nguyen et al., 2019)

$$\varepsilon = \frac{1}{2}\left(\nabla u + \nabla u^T + \nabla u.\nabla u^T\right) \tag{11}$$

where

$$\begin{Bmatrix} \varepsilon_{xx} \\ \varepsilon_{zz} \\ \varepsilon_{xz} \end{Bmatrix} = \begin{Bmatrix} u_{,x} + \frac{1}{2}(w_{,x})^2 \\ w_{,z} + \frac{1}{2}(w_{,z})^2 \\ \frac{1}{2}\left[u_{,z} + w_{,x}(1 + w_{,z})\right] \end{Bmatrix} \tag{12}$$

where it is presumed that the strain tensor follows symmetrical rules as $\varepsilon_{ij} = \varepsilon_{ji}$.

Maxwell's equation can be fulfilled by treating the combination of a cosine and a linear function to reach us with the distribution of the electric potential as (Malikan, 2018; Malikan, 2019; Malikan, 2017; Su et al., 2018)

$$\Phi(x,y,z) = -\cos(\beta z)\phi(x,y) + \frac{2zV_0}{h} \tag{13}$$

where $\beta = \pi/h$; V_0 is external electric voltage; ϕ is the electric potential's magnitude in the mid-plane; $\Phi$is the electric potential function.

The components of the electric field can be written as

$$\begin{bmatrix} d_x & d_y & d_z \end{bmatrix}^T = -\begin{bmatrix} \Phi_{,x} & \Phi_{,y} & \Phi_{,z} \end{bmatrix}^T \tag{14}$$

Eq. (8) can be re-shown in the simpler status as (Stempin et al., 2023).

$$\delta W - \delta U = 0 \tag{15}$$

The variations of the strain energy can be categorized into mechanical and electrical forms for the present study as

$$\delta U = \delta U^{Mechanical} + \delta U^{Electrical} \tag{16}$$

Further, the non-zero tensors can be collected to derive both aforementioned parts as (Wang and Xu, 2010)

$$\delta U = \frac{1}{2}\int_V [\sigma\delta\varepsilon - D\delta d]dV = 0 \tag{17}$$

The work done by external loads includes the influence of the lateral static load and the electric field (Nguyen et al., 2019)

$$\delta W = \frac{1}{2}\int_0^L \left[N_{xx}^0(\delta w)_{,x}w_{,x}\right]dx \tag{18}$$

where $N_{xx}^0 = 2\bar{e}_{31}V_0/h$ is an in-plane electric force.

It should be noted that the energy of body forces is neglected in this study. Then, we establish the nonlinear dynamic governing equations by operating the variational technique on Eqs. (17) and (18), supposing a 3D beam-like structure neglecting the changes in the y-axis. In this regard, one attains

$$\sigma_{xx,x} + \tau_{xz,z} = 0 \tag{19a}$$

$$\sigma_{xx,x}w_{,x} + \sigma_{zz,z}(1 + w_{,z}) + \sigma_{xx}w_{,xx} + \sigma_{zz}w_{,zz} + \tau_{xz,x}(1 + w_{,z}) + \tau_{xz,z}w_{,x} + 2\tau_{xz}w_{,xz} + N_{xx}^0 w_{,xx} = 0 \tag{19b}$$

$$\widehat{D}_{x,x} + \widehat{D}_z = 0 \tag{19c}$$

where

$$\widehat{D}_x = \int_{-h/2}^{h/2} D_x \cos(\beta z) dz, \widehat{D}_z = \int_{-h/2}^{h/2} D_z \beta \sin(\beta z) dz.$$

The analytical boundary conditions derived from the variational technique become arranged as

$$\begin{aligned} \delta U^{Mechanical} &= -\int \left[\sigma_{xx}\delta u + \tau_{xz}\delta w + \sigma_{xx} w_{,x}\delta w + \tau_{xz} w_{,z}\delta w\right] dz \\ &- \int \left[\sigma_{zz}\delta w + \tau_{xz}\delta u + \sigma_{zz} w_{,z}\delta w + \tau_{xz} w_{,x}\delta w\right] dx \end{aligned} \tag{20a}$$

$$\delta U^{Electrical} = \int [\widehat{D}_x]\delta\phi dz \tag{20b}$$

Evidently, Eq. (19c) causes a problem in the 3D studies due to the inclusion of the definite integral through the thickness. In the 3D mechanical analyzes, the thickness is supposed to be variable after deformation. This is the fact that the undertook process cannot be put to use for 3D evaluations. Therefore, let us comply with Eq. (10) and deal with the 3D piezoelectricity to deduce the following electric potential

$$\Phi(x, y, z) = \psi(x, y, z) \tag{21}$$

in which $\psi$is the 3D electric potential's magnitude.

It means that there is no premise similar to Eq. (13) for electric potential distribution.

The comprisal of the electric potential leads to

$$\delta\psi = 0; D_{x,x} + D_{z,z} = 0 \tag{22}$$

where this equation is free of the obstacle that we faced earlier by Eq. (19c).

From this point forward, there are two ways to obtain a solution. One can solve three equations, Eqs. (19a), (19b), and (22) with three unknown variables (u, w, and ψ). However, defining any shape function for ψ cannot provide us with accurate results as the electric surface conditions must be satisfied. The other way could be finding an expression for electric potential achieved by Eq. (22) as

$$\begin{aligned} \Phi = \left(\frac{h^2}{8} - \frac{z^2}{2}\right) &\left[\frac{\overline{e}_{15}}{\overline{\kappa}_{33}}\left(u_{,xz} + w_{,xx} + w_{,xx}w_{,z} + w_{,x}w_{,xz}\right) + \frac{\overline{e}_{31}}{\overline{\kappa}_{33}}\left(u_{,xz} + w_{,x}w_{,xz}\right)\right. \\ &\left. + \frac{\overline{e}_{33}}{\overline{\kappa}_{33}}\left(w_{,zz} + w_{,z}w_{,zz}\right)\right] + V_0\left(\frac{z}{h} + \frac{1}{2}\right) \end{aligned} \tag{23}$$

The surface conditions ($\Phi(+h/2, -h/2) = \{V_0, 0\}$) regarding the electric voltage can be contented using Eq. (23) as well.

The analytic electrical boundary conditions can be presented by Eq. (24) in a replacement of Eq. (20b).

$$\delta U^{Electrical} = -\left[\int D_x \delta\psi dz + \int D_z \delta\psi dx\right] \tag{24}$$

Eventually, in order to encounter electro-elastic deflections, Eq. (19a) and (19b) are sufficient to be taken in the solving process.

The stress and strain tensors have been given symmetrical; however, it has nothing to do with the elastic stiffness matrix being symmetrical or non-symmetrical. Nevertheless, it helped to decrease the needed constants. To access the symmetrical elastic stiffness matrix ($C_{ijkl} = C_{jikl} = C_{ijlk} = C_{klij}$), there exists a reduced number of independent constants on the basis of the Voigt notation and converted into $C_{\alpha\beta}$ ($\alpha, \beta \in \{1, 2, \ldots, 6\}$). On this condition, the material is supposed to possess a plane of linear elastic symmetry consisting of transversely isotropic behavior (however, the electro-mechanical constants are being defined in a fully orthotropic form) (Zhou et al., 2021)

$$[C] = \begin{bmatrix} \overline{C}_{1111} & \overline{C}_{1122} & \overline{C}_{1133} & 0 & 0 & 0 \\ \overline{C}_{1122} & \overline{C}_{2222} & \overline{C}_{2233} & 0 & 0 & 0 \\ \overline{C}_{1133} & \overline{C}_{2233} & \overline{C}_{3333} & 0 & 0 & 0 \\ 0 & 0 & 0 & \overline{C}_{2323} & 0 & 0 \\ 0 & 0 & 0 & 0 & \overline{C}_{1313} & 0 \\ 0 & 0 & 0 & 0 & 0 & \overline{C}_{1212} \end{bmatrix} \tag{25}$$

The piezoelectric tensor can be presented for hexagonal perovskite piezoelectric crystalline materials using the Voigt notation as (Li et al., 2020)

$$[e]=\begin{bmatrix}0&0&0&0&\overline{e}_{113}&0\\0&0&0&\overline{e}_{223}&0&0\\\overline{e}_{311}&\overline{e}_{322}&\overline{e}_{333}&0&0&0\end{bmatrix} \tag{26}$$

where the piezoelectric constants were transformed from e_{ijk} into $e_{i\alpha}$ ($\alpha \in \{1, 2, \ldots, 6\}$).

The fully 3D electro-elastic stress-strain constitutive relations (Eq. (3)) can be evolved as follows

$$\begin{Bmatrix}\sigma_{xx}\\\sigma_{yy}\\\sigma_{zz}\\\tau_{yz}\\\tau_{xz}\\\tau_{xy}\\D_x\\D_y\\D_z\end{Bmatrix}=\begin{bmatrix}\overline{C}_{1111}&\overline{C}_{1122}&\overline{C}_{1133}&0&0&0\\\overline{C}_{2211}&\overline{C}_{2222}&\overline{C}_{2233}&0&0&0\\\overline{C}_{3311}&\overline{C}_{3322}&\overline{C}_{3333}&0&0&0\\0&0&0&\overline{C}_{2323}&0&0\\0&0&0&0&\overline{C}_{1313}&0\\0&0&0&0&0&\overline{C}_{1212}\\0&0&0&0&\overline{e}_{113}&0\\0&0&0&\overline{e}_{223}&0&0\\\overline{e}_{311}&\overline{e}_{322}&\overline{e}_{333}&0&0&0\end{bmatrix}\begin{Bmatrix}\varepsilon_{xx}\\\varepsilon_{yy}\\\varepsilon_{zz}\\\gamma_{yz}\\\gamma_{xz}\\\gamma_{xy}\end{Bmatrix}+\begin{bmatrix}0&0&\overline{e}_{311}\\0&0&\overline{e}_{322}\\0&0&\overline{e}_{333}\\0&\overline{e}_{223}&0\\\overline{e}_{113}&0&0\\0&0&0\\-\overline{\kappa}_{11}&0&0\\0&-\overline{\kappa}_{22}&0\\0&0&-\overline{\kappa}_{33}\end{bmatrix}\begin{Bmatrix}\Phi_{,x}\\\Phi_{,y}\\\Phi_{,z}\end{Bmatrix} \tag{27}$$

The reduced coupling components of the symmetric stiffness matrix for a 3D linear elastic material can be defined as (Affdl and Kardos, 1976; Dastjerdi and Akgöz, 2018; Komijani et al., 2014)

Elastic constants:

$$\begin{aligned}&\overline{C}_{1111}=C_{1111}-\frac{C_{1133}C_{3311}}{C_{3333}},\overline{C}_{1122}=C_{1122}-\frac{C_{1133}C_{3322}}{C_{3333}},\\&\overline{C}_{1133}=C_{1122}-\frac{C_{1133}C_{1133}}{C_{3333}},\overline{C}_{2222}=C_{2222}-\frac{C_{2233}C_{3322}}{C_{3333}},\\&\overline{C}_{2211}=\overline{C}_{1122},\overline{C}_{1133}=\overline{C}_{3311},\overline{C}_{2323}=C_{2323},\overline{C}_{1313}=C_{1313},\\&\overline{C}_{1212}=C_{1212},\overline{C}_{3333}=\overline{C}_{1111}\end{aligned} \tag{28a}$$

Piezoelectric constants:

$$\begin{aligned}&\overline{e}_{311}=e_{311}-\frac{C_{1133}e_{333}}{C_{3333}},\overline{e}_{322}=e_{322}-\frac{C_{2233}e_{333}}{C_{3333}},\\&\overline{e}_{333}=e_{333},\overline{e}_{113}=e_{113},\overline{e}_{223}=e_{223}\end{aligned} \tag{28b}$$

Dielectric constants:

$$\overline{\kappa}_{11}=\kappa_{11},\overline{\kappa}_{22}=\kappa_{22},\overline{\kappa}_{33}=\kappa_{33}+\frac{e_{333}e_{333}}{C_{3333}} \tag{28c}$$

where the pure elastic constants can be given for an orthotropic material as (Affdl and Kardos, 1976)

$$\begin{bmatrix}C_{1111}\\C_{1122}\\C_{2222}\\C_{2233}\\C_{3333}\\C_{3311}\end{bmatrix}=\begin{bmatrix}\eta E_x\left(1-\nu_{yz}\nu_{zy}\right)\\\eta E_y\left(\nu_{xy}+\nu_{xz}\nu_{zy}\right)\\\eta E_y\left(1-\nu_{xz}\nu_{zx}\right)\\\eta E_z\left(\nu_{yz}+\nu_{yx}\nu_{xz}\right)\\\eta E_z\left(1-\nu_{xy}\nu_{yx}\right)\\\eta E_x\left(\nu_{zx}+\nu_{zy}\nu_{yx}\right)\end{bmatrix} \tag{29a}$$

$$\begin{bmatrix}C_{2323}\\C_{1313}\\C_{1212}\end{bmatrix}=\begin{bmatrix}G_{yz}\\G_{xz}\\G_{xy}\end{bmatrix}=\begin{bmatrix}\dfrac{E_yE_z}{E_y+E_z+2E_z\nu_{yz}}\\\dfrac{E_xE_z}{E_x+E_z+2E_z\nu_{xz}}\\\dfrac{E_xE_y}{E_x+E_y+2E_y\nu_{xy}}\end{bmatrix} \tag{29b}$$

in which

$$\eta=\frac{1}{1-\nu_{xy}\nu_{yx}-\nu_{yz}\nu_{zy}-\nu_{zx}\nu_{xz}-\nu_{xy}\nu_{yz}\nu_{zx}-\nu_{yx}\nu_{xz}\nu_{zy}}.$$

We must ensure that the following symmetry rules will not be violated when the 3D material properties are input.

$$\begin{aligned}&\nu_{yz}E_z=\nu_{zy}E_y\\&\nu_{xz}E_z=\nu_{zx}E_x\\&\nu_{xy}E_y=\nu_{yx}E_x\end{aligned} \tag{30}$$

2.2. FGMs-based nanocomposites

In order to model functionally graded nanocomposite structures enriched with nanoparticles such as graphene nanoplatelets, 2D nanofillers, etc., there are several well-used micro-mechanic mixtures (Eyvazian et al., 2020; Karami and Ghayesh, 2024) where the Halpin-Tsai is here taken into formulations to calculate the elasticity and electrical features of the nanocomposite. Nevertheless, despite of accuracy of the model, the dispersed GNPs wt% shall not exceed the specific value of 1%. The reason is if the composite contains bigger values of GNPs wt%, its fracture toughness becomes lower (Shokrieh et al., 2014).

The patterns of GNPs used within this study are limited to U (UD), X (FG-X), and O (FG-O) shown in Fig. 3 in which the detailed distributions of the GNPs in each layer for the X and O patterns can be witnessed. The construction of Fig. 3 is in a way that the darker the color, the more the GNPs vol.%. Thus, for the X pattern, the highest richness of the GNPs is regarding the top and bottom layers. The average of the GNPs vol.% for the FG-X is the same as the UD (0.3%). For the U pattern, the GNPs wt% keeps the same amount in each layer through the entire layers which means the UD is just a uniform nanocomposite with a lack of FGM concept.

The graphene nanoplatelets' volume fractions (g^*_{gnp}) in the k-th layers ($g^{(k)}_{gnp}$) can be expressed as the following items for the U, O, and X composition patterns (Ebrahimi and Dabbagh, 2019; Malekzadeh et al., 2018; Malikan et al., 2017; Nguyen and Lee, 2021; Ninh et al., 2022; Rafiee et al., 2014; Saidi et al., 2019; Tabatabaei-Nejhad et al., 2020)

UD:

$$g^{(k)}_{gnp} = g^*_{gnp} \tag{31}$$

FG-X:

$$g^{(k)}_{gnp} = 4g^*_{gnp}\left(\frac{1}{2}+\left|k-\frac{N_L+1}{2}\right|\right)\Big/(2+N_L) \tag{32}$$

FG-O:

$$g^{(k)}_{gnp} = 4g^*_{gnp}\left(\frac{N_L+1}{2}-\left|k-\frac{N_L+1}{2}\right|\right)\Big/(2+N_L) \tag{33}$$

where $N_L$is the number of layers in FGM.

The effective elasticity modulus of the k-th layer of the FGM can be expressed as

$$E^{(k)}_j = \frac{3}{8}\left(\frac{1+\xi_L\eta_L V^{(k)}_{gnp}}{1-\eta_L V^{(k)}_{gnp}}\right)\times E_j + \frac{5}{8}\left(\frac{1+\xi_T\eta_T V^{(k)}_{gnp}}{1-\eta_T V^{(k)}_{gnp}}\right)\times E_j; j = x, z \tag{34}$$

in which

$$V^{(k)}_{gnp} = \frac{g^{(k)}_{gnp}}{g^{(k)}_{gnp} + (\rho_{gnp}/\rho_m)\left(1-g^{(k)}_{gnp}\right)} \tag{35}$$

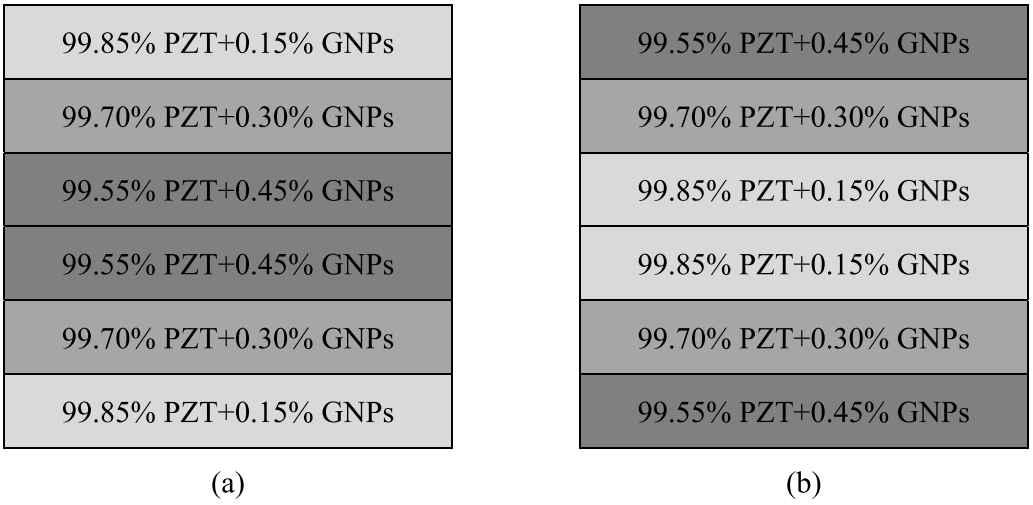

Fig. 3. The distribution patterns of graphene nanoplatelets in line with the z-axis for 0.3wt%; (a) O-type FGM, (b) X-type FGM.

$$\eta_L = \frac{\left(E_{gnp}/E_j\right) - 1}{\left(E_{gnp}/E_j\right) + \xi_L},\ \eta_T = \frac{\left(E_{gnp}/E_j\right) - 1}{\left(E_{gnp}/E_j\right) + \xi_T} \tag{36}$$

and

$$\xi_L = 2\left(\frac{a_{gnp}}{h_{gnp}}\right),\ \xi_T = 2\left(\frac{b_{gnp}}{h_{gnp}}\right) \tag{37}$$

where the average length, thickness and width of GNPs can be defined by a_{gnp}, h_{gnp} and b_{gnp}, respectively.

Eq. (34) generates elasticity modulus for x and z directions for each virtual layer only. All the layers of the FGM should be substituted by one solid layer according to the laminate theory.

The rule of mixture can determine the dielectric and piezoelectric constants, the Poisson's ratio, and the mass density as follows (Komijani et al., 2014)

$$\rho^{(k)} = \rho_{gnp} V_{gnp}^{(k)} + \rho_M V_M^{(k)} \tag{38a}$$

$$\nu_{ij}^{(k)} = \nu_{gnp} V_{gnp}^{(k)} + \nu_{ij} V_M^{(k)}; i,j = x,y \tag{38b}$$

$$e_{km}^{(k)} = e_{km,gnp} V_{gnp}^{(k)} + e_{km,M} V_M^{(k)} \tag{38c}$$

$$\kappa_{km}^{(k)} = \kappa_{km,gnp} V_{gnp}^{(k)} + \kappa_{km,M} V_M^{(k)} \tag{38d}$$

where $V_M^{(k)} = \left(1 - V_{gnp}^{(k)}\right)$.

3. GDQ numerical technique

The Generalized Differential Quadrature (GDQ) method is a highly efficient numerical technique that has been successfully used to solve mechanical problems based on ordinary and partial differential equations (Dastjerdi and Jabbarzadeh, 2017; Dastjerdi and Jabbarzadeh, 2016; Dastjerdi et al., 2016; Jena et al., 2021; Malikan and Sadraee Far, 2018). GDQ has several advantages over other solution procedures. It can provide mechanical information on any point of a domain, ranging from displacements to stresses, in light of the grid point. Moreover, because of taking on the polynomial terms, GDQ permits a fast convergence. In addition to this, GDQ owns a non-uniform grid point that causes more precise results at the boundaries. Such benefits cannot be seen in available solution techniques (Barretta et al., 2024; Farokhi and Ghayesh, 2018; Farokhi et al., 2017; Ghayesh, 2011; Mirfatah et al., 2024; Shariff and Bustamante, 2024; Malikan and Eremeyev, 2023), although they are accurate, error-free, and well-established. We here carry out the GDQ and apply it to the obtained governing equations to indicate a parametric study providing the numerical results.

The satisfaction of the corresponding boundary conditions (BCs) must be ensured to fix the problem. Herein, various types of the BCs can be achieved.

- Clamped/fixed edges (C):

$$u\big|_{x=0,L} = w\big|_{x=0,L} = 0$$

- Simply-supported edges (S):

$$w\big|_{x=0,L} = \sigma_{xx}\big|_{x=0,L} = 0$$

- Free edges (F):

$$\sigma_{xx}\big|_{x=0,L} = \tau_{xz}\big|_{z=-h/2,+h/2} = 0$$

Since the study grants a 3D domain, the topmost and lowermost surfaces of the thickness are involved with the following conditions
Top: $\sigma_{zz}\big|_{z=+h/2} = q/b, \tau_{xz}\big|_{z=+h/2} = 0$; where q defines the transverse static load.
Bottom: $\sigma_{zz}\big|_{z=-h/2} = \tau_{xz}\big|_{z=-h/2} = 0$
The electric BCs are categorized into two cases (Wankhade and Bajoria, 2013)

$$\text{Open} - \text{circuit (sensor)}: \ \Phi = 0 \text{ at } z = -h/2, +h/2 \tag{39a}$$

$$\text{Closed}-\text{circuit (actuator)}: \begin{cases} \Phi = V_0 \text{ at } z = +h/2 \\ \Phi = 0 \text{ at } z = -h/2 \end{cases} \tag{39b}$$

where the closed-circuit is investigated in this paper only. Briefly, in order to fabricate actuators and ultrasonic motors, the close-circuit piezoelectric structures are mostly used. Also, in order to design frequency sensors, an open-circuit piezoelectric structure is employed.

With respect to the satisfied types of BCs and the applied function, several subsets can be the subdivision of the GDQM. To this end, in this work, direct substitution techniques together with the polynomial function are utilized. Therefore, the derivatives of a function F_0 in the first-order forms in the rectangular coordinate can be defined as

$$\frac{\partial F_0(x_i, z_j)}{\partial x} = \sum_{k=1}^{M_x} a_{ik}^x u(x_k, z_j) i = 1, 2, \ldots, M_x \tag{40a}$$

$$\frac{\partial F_0(x_i, z_j)}{\partial z} = \sum_{r=1}^{M_z} a_{jk}^z u(x_i, z_r) j = 1, 2, \ldots, M_z \tag{40b}$$

where a^x and a^z can be obtained as

$$\left| \begin{array}{l} a_{ij}^x = \dfrac{R(x_i)}{(x_i - x_j)R(x_j)} \text{for} i \neq j \\ a_{ii}^x = -\sum\limits_{j=1,\neq i}^{M_x} a_{ij}^x, i, j = 1, 2, \ldots, M_x \end{array} \right| \quad \left| \begin{array}{l} a_{ij}^z = \dfrac{R(z_i)}{(z_i - z_j)R(z_j)} \text{for} i \neq j \\ a_{ii}^z = -\sum\limits_{j=1,\neq i}^{M_z} a_{ij}^z, i, j = 1, 2, \ldots, M_z \end{array} \right| \tag{41a,b}$$

in which$R(x_i)$ and then $P(x_i)$ become

$$\left| \begin{array}{l} R(x_i) = \prod\limits_{j=1,\neq i}^{M_x} (x_i - x_j) \\ P(z_i) = \prod\limits_{j=1,\neq i}^{M_z} (z_i - z_j) \end{array} \right| \tag{42}$$

The higher-order partial derivatives are also calculated by

$$\frac{\partial^{(n)} F_0(x_i, z_j)}{\partial x^{(n)}} = \sum_{k=1}^{M_x} C_{ik}^{(n)} F_0(x_k, z_j) \tag{43a}$$

$$\frac{\partial^{(m)} F_0(x_i, z_j)}{\partial x^{(m)}} = \sum_{r=1}^{M_z} C_{jr}^{(m)} F_0(x_i, z_r) \tag{43b}$$

$$\frac{\partial^{(l+s)} F_0(x_i, z_j)}{\partial x^{(l)} \partial z^{(s)}} = \sum_{k=1}^{M_x} \sum_{r=1}^{M_z} C_{ik}^{(l)} \overline{C}_{jr}^{(s)} F_0(x_k, z_r) \tag{43c}$$

in which the $\overline{C}$ and C parameters denote the weighting coefficients in line with the z and x axes. Also, the order of derivatives is shown by the superscripts (m, n, l, and s). Then

$$C^{(1)} = a^x, \overline{C}^{(1)} = a^z \tag{44}$$

$$\left| \begin{array}{l} C_{ij}^{(n)} = n\left[a_{ij}^x C_{ii}^{(n-1)} - \dfrac{C_{ij}^{(n-1)}}{x_i - x_j}\right] \text{for} i \neq j \\ C_{ii}^{(n)} = -\sum\limits_{j=1,\neq i}^{M_x} C_{ij}^{(n)} i, j = 1, 2, \ldots, M_x \end{array} \right| , \quad \left| \begin{array}{l} \overline{C}_{ij}^{(m)} = m\left[a_{ij}^z \overline{C}_{ii}^{(m-1)} - \dfrac{\overline{C}_{ij}^{(m-1)}}{z_i - z_j}\right] \text{for} i \neq j \\ \overline{C}_{ii}^{(m)} = -\sum\limits_{j=1,\neq i}^{M_z} \overline{C}_{ij}^{(m)} i, j = 1, 2, \ldots, M_z \end{array} \right| \tag{45a,b}$$

In what follows, the well-known Chebyshev-Gauss-Lobatto grid point is taken for the domain throughout the x and z-axes (Malikan, 2024)

$$x_i = \frac{1}{2} L\left[1 - \cos\left(\frac{i-1}{M_x - 1}\pi\right)\right], i = 1, 2, \ldots, M_x \tag{46a}$$

$$z_k = \frac{1}{2}h\cos\left(\frac{k-1}{M_z-1}\pi\right), k = 1, 2, ..., M_z \tag{46b}$$

in which M_x and M_z are the maximum number of points in each direction.

Fig. 4 is a schematic representation of grid points on the domain on which the 3D deformation properties such as thickness stretching can be obtained as far as the points move separately but dependently. The colors associated with each point mean different situations, namely the boundaries of the domain are defined by solid black points and the solid blue points obey governing equations.

4. Validation

The above-developed methodologies can be verified in this section. Initially, it is germane to note that the GDQ numerical results converge at 9 × 9 points, leading to the most precise results. As far as the commercial FEM codes are unable to model smart and multifunctional composites properly and meticulously (to the best of the authors' knowledge), a 3D thick beam built from a steel alloy with the below properties has been taken into validation in Abaqus software:

$$E = 190\text{GPa},\ \nu = 0.29,\ h = 8\text{cm},\ b/h = 1,\ L/h = 2.5,\ q = 0.1\text{GPa},\ \text{CC}.$$

Respectively, Fig. 5 calculated the path of deformations through the thickness of the beam in FEM and GDQM. In addition to this, by presenting Fig. 6, maximum deflections have been computed for the beam in the present method in comparison with the Abaqus. It should be borne in mind that the maximum deflection here and beyond is not the same as mid-plane deflection and the meaning of the maximum deflection is the transverse displacement of the topmost surface as a result of thickness change, plus mid-span displacement which is peculiar for 3D analyzes. As observed, an excellent agreement between the results of both methods can be identified. This approval lets us create a parametric study and discuss it in detail in the next section.

5. Results and discussions

The main discussion of this section relates to a smart composite which is made in different modes. The main structure and desired matrix of PZT-5H piezoelectric material are considered, which is due to its excellent electrical properties compared to PZT-5A, PZT-5J, and PZT-4 piezoelectric structures. Generally, PZT-5A suits a vast varying temperature and extreme heat but does not have desirable electrical features. In addition, PZT-5H consists of the best piezo characteristics. On the other side, PZT-5J could be in between 5A and 5H. Further, although PZT-4′s electrical properties are comparable with PZT-5H, it is a little less sensitive (Ke et al., 2015; Prolongo et al., 2014).

The smart composite is in the forms of FGM with X composition (FG-X), FGM with O composition (FG-O), uniform composite (UD), and PZTC pure structure, in which graphene nanoplatelets (GNPs) are used in the first to third structure to strengthen the matrix. GNPs are supposed as square plates with a perfect geometry. Considering the thickness of graphene sheets (0.34 nm), the thickness of GNPs is considered to be 20 layers for almost all results. The length and width of graphene platelets are considered to be 100 nanometers. Since the volumetric percentage of graphene nanoplatelets plays an essential role in the behavior of the designed smart composite, its value is 0.3 percent in most results. Moreover, the transverse static load is also assumed to be 0.1GPa in order to extract the results. Also, the dimensions of the medium are considered as 8 × 8 × 20 cm^3. This size is associated to the parametric study and is not related to a specific sensor or actuator. Furthermore, the height of layers is assumed identical in undeformed beams. More importantly, the mechanical properties of the piezoelectric matrix have to be tabulated by the elastic modulus and Poisson's ratio, not via components of the stiffness elastic matrix. The reason is their necessity in the micro-mechanic model. Plus to this, the density of PZT-5H is also 7500 kg/m^3 for documentation purposes. The full material properties of the PZT-5H and GNPs can be seen by Table 1.

First, we present a comparison for the mechanical response of the four structures set here, namely, FG-X, FG-O, UD, and PZTC by making visual data as prepared in Fig. 7a and b. The principle difference is that in Fig. 7a, the transverse load is eliminated and the composite beams are located in an electrical field influenced by an external electric voltage. Contrasting between the two figures

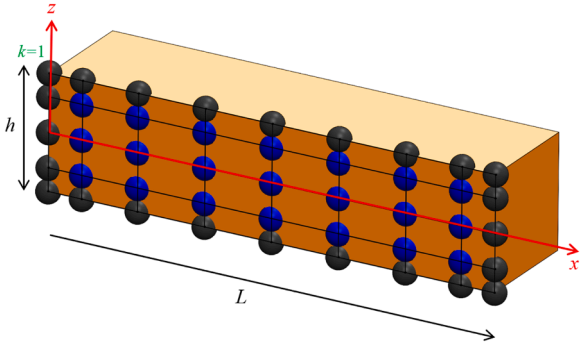

Fig. 4. GDQ grid points of the symmetrical beam for two directions ($M_x = 9$, $M_z = 5$).

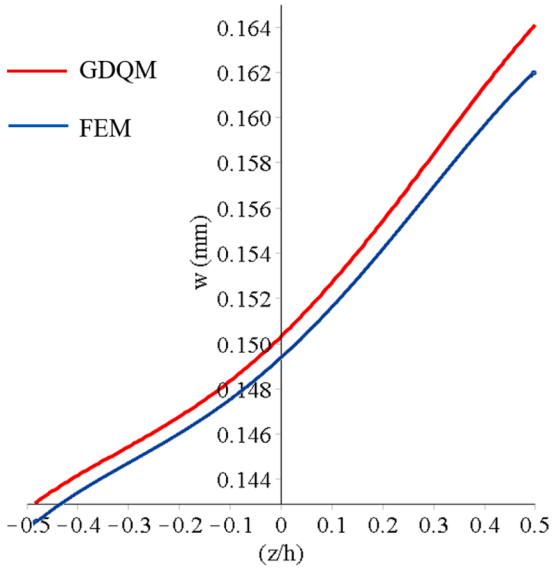

Fig. 5. The path of transverse displacements in line with the thickness.

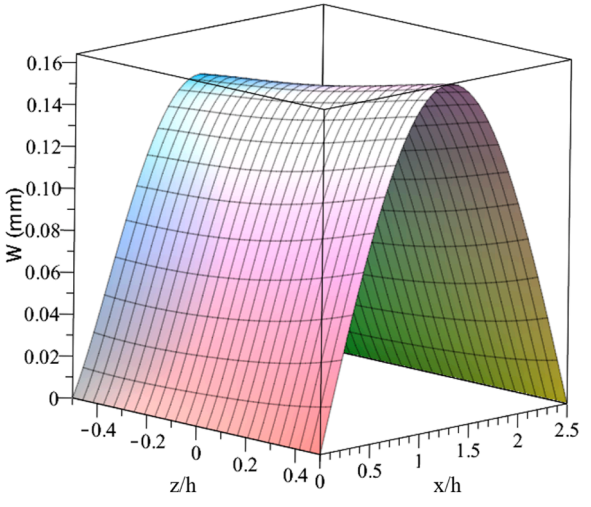

Fig. 6. Deflections by GDQM drawn in Maple.

Table 1
Full material properties of the smart nanocomposite beam (ABC n.d.; Alshenawy et al., 2023; Prolongo et al., 2014; Zhou et al., 2021).

PZT-5H
Mechanical constants: $E_x = 60.61$ GPa, $E_y = 60.61$ GPa, $E_z = 48.31$ GPa, $\nu_{xy} = 0.289$, $\nu_{xz} = 0.512$, $\nu_{yz} = 0.512$ Piezoelectric constants: $e_{15} = 17$ C/m^2, $e_{24} = e_{15}$, $e_{31} = -6.5$ C/m^2, $e_{32} = e_{31}$, $e_{33} = 23.3$ C/m^2 Dielectric constants: $\kappa_{11} = 1.505 \times 10^{-8}$ C/V.m, $\kappa_{22} = 1.505 \times 10^{-8}$ C/V.m, $\kappa_{33} = 1.302 \times 10^{-8}$ C/V.m
GNPs
$E_{gnp} = 1010$ GPa, $\nu_{gnp} = 0.186$, $\rho_{gnp} = 1920$ kg/m^3, $a = 100$nm, $b = 100$nm, $h = 6.8$nm (20Layers)

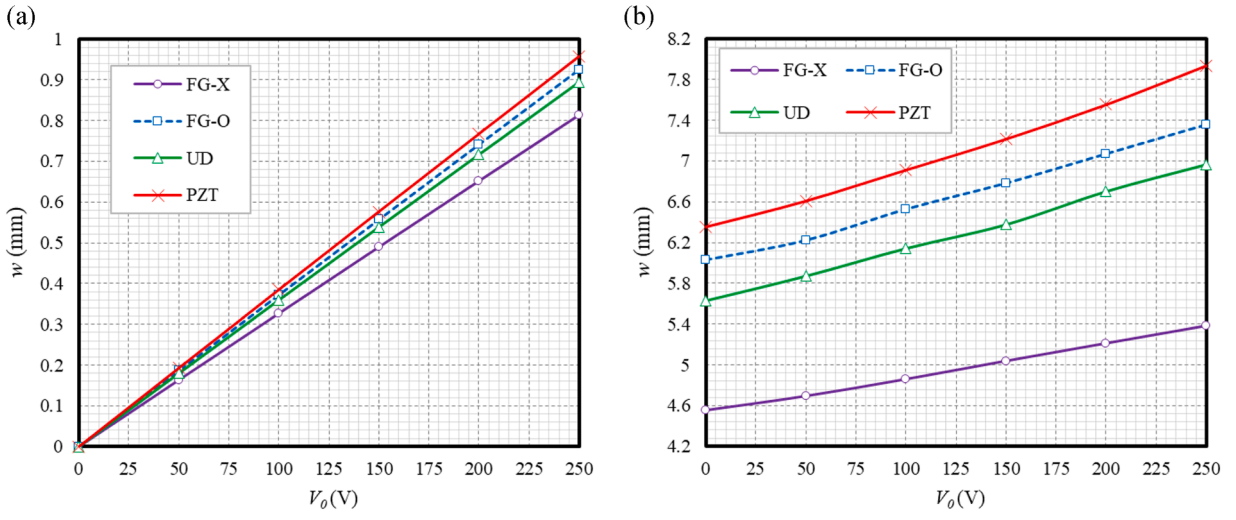

Fig. 7. a External electric voltage vs. various beam mixtures ($q = 0$). b External electric voltage vs. various beam mixtures ($q = 0.1$ GPa).

indicates that the FG-X type has the highest mechanical properties and the most strength structure among the aforementioned ones due to its least static deflections in both figures. In the first figure, because of the lack of transverse static load, when the external electric voltage is neglected ($V_0 = 0$), the deflections are equal to zero; however, the figure shows deflections at $V_0 \neq 0$ that are caused by the electric field. The deflections in Fig. 7b belong to both lateral static force and the electric voltage. This achievement pertains to the three-dimensional electro-elastic analysis. If one uses beam theories (1D), the absence of mechanical loads leads to $w = 0$ even if an electrical field surrounds the matrix. Based on these results, it is also demonstrated that making FGM cannot assure us with the best results and UD gives a better mechanical performance than FG-O. So, the layout of the FGM layers is decisive not the FGM itself.

In order to warrant a comparison of results, Table 2 is prepared to supply numeric data based on the results of Fig. 7a and b.

One of the initial and at the same time the most influential factors in investigating the present issue is the volume percentage of GNPs (wt%) in the three designed composite structures considered in Fig. 8. This volume percentage, as explained in the previous sections, according to scientific research background, is better to do not exceed 1%. Because graphene is a relatively brittle material, an amount greater than this value leads to easier fragility of the final composite structure. The zero value indicates the absence of graphene in all the structures and therefore the results are the same at zero value for wt%. The pure structure of PZTC is also not affected by the amount of GNPs, and hence the results of the mechanical behavior of PZTC can be seen as a straight line. One can see that the greatest effect of graphene is on X-type composite and this kind of FGM is greatly influenced by the increase in GNPs' volume percentage. The result could be on the ground of the outer layers. Upon the further GNPs' percentage in the outmost layers, these layers will have more material stiffness then enable the beam to carry higher bending moments. From the classic strength of material, it has been known that a hollow pipe with the same mass of a solid pipe, could have more stiffness. Its mass is concentrated on the outside, leading to larger moment of inertia which results in further bending stiffness. This is the fundamental reason for such an achievement in X-type FGM.

Among the parameters that affect the mechanical behavior of the analyzed structures, especially for the two modes of FGM namely X and O, the number of virtual layers is here considered for the design of FGM intelligent composite material. This fact is the purpose of presenting Fig. 9. On the horizontal axis of this figure, it is quite clear that the number of layers is postulated to be varied from 4 to 20.

Table 2
External electric voltage vs. various compositions of the beam-like nanocomposite.

q (GPa)	V_0 (V)	Maximum deflections (mm)			
		FG-X	FG-O	UD	PZT
0	0	0	0	0	0
	50	0.1640047	0.1865247	0.1803922	0.1930458
	100	0.3273885	0.3722470	0.3600336	0.3852325
	150	0.4901577	0.5571763	0.5389328	0.5765706
	200	0.6523180	0.7413220	0.7170981	0.7670704
	250	0.8138781	0.9246934	0.8945381	0.9567423
0.1	0	4.5527843	6.0313012	5.6272566	6.3500854
	50	4.6926560	6.2239391	5.8702493	6.6055489
	100	4.8585649	6.5284000	6.1416815	6.9098712
	150	5.0377225	6.7823032	6.3770290	7.2153112
	200	5.2111600	7.0701030	6.7023224	7.5545156
	250	5.3823437	7.3559271	6.9672257	7.9372336

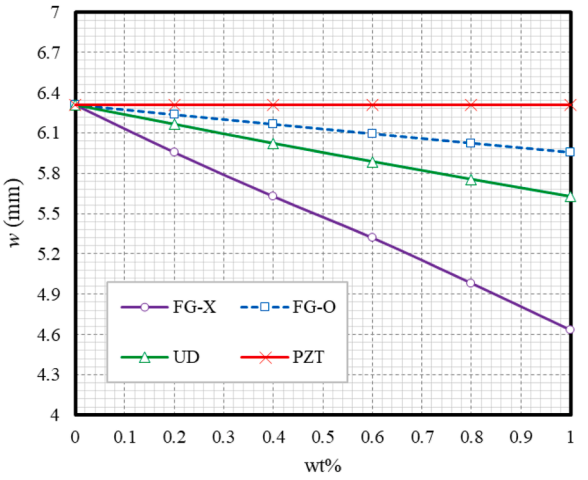

Fig. 8. GNPs' volume fraction vs. various beam mixtures.

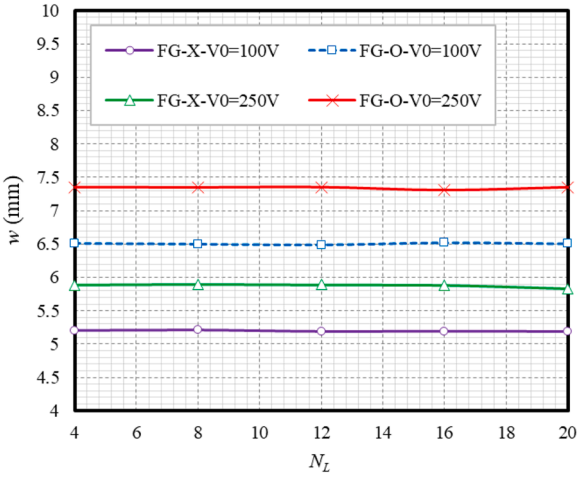

Fig. 9. FGM's number of layers vs. electric voltage.

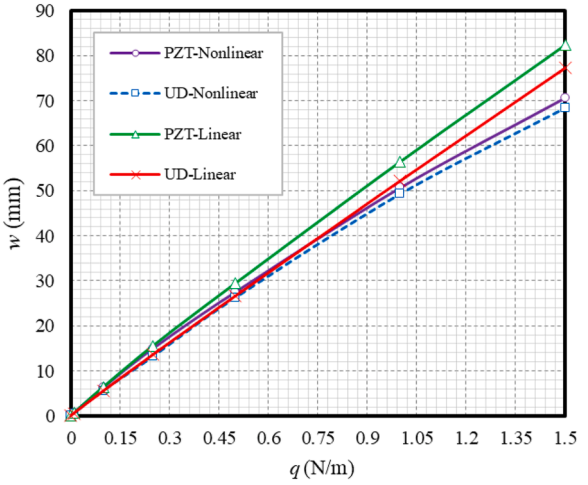

Fig. 10. Lateral load vs. geometrical nonlinearity.

Although here the increase or decrease in the number of layers has very little impact on the electro-elastic behavior of FGM structures, it is necessary to note that the effect of changing the number of layers could be more prominent in the values of the elastic modulus than the deflection results.

The effect of the amount of the mechanical load should be evaluated and it has an important and vital role in the values of deflections and mechanical behavior of assumed composite materials. As a matter of fact, the value of this load relatively determines whether the behavior of the structure is linear or nonlinear. Accurately, even if the nonlinear elastic strains are calculated, the relative small amount of static bending load causes a linear mechanical response. Therefore, both linear and nonlinear modes for two different materials are shown with the aid of Fig. 10. It should be noted that since we are dealing with the three-dimensional analysis of the beam, the unit of mechanical load is Newton per meter. With the help of this figure, it has been shown that after $q = 1\text{GPa}$, the results of linear and nonlinear deflections start to extremely diverge from each other.

Figs. 11, 12, 13, and 14 are represented to show the deformation and deflection values along the thickness. These four figures express the three-dimensional solution of the problem. Otherwise, in the one-dimensional solution of beams by means of beam theories, it is not possible to calculate the deformation of the thickness and the deflection has the same value at all points of the thickness. Exact three-dimensional electro-elastic analysis has opened this path for us to obtain valuable results in the field of mechanics of intelligent composite structures by examining the real and different values of deflections at each point along the thickness of the beam. In the next figures, the variable of the problem is, respectively, for Fig. 11 electric voltage, for Fig. 12 different beam structures, for Fig. 13 the number of different layers for GNPs and thus different thicknesses, and finally for Fig. 14 different volume percentage for GNPs have been taken into analyzes.

Fig. 11 illustrates various values of the external electric voltage. As seen, these values influence not only the maximum deflections but also the way that the thickness deforms. The literature widely confirms that the amount of external electric voltage impresses the maximum deflections. Nevertheless, here, through a full 3D analysis, we recognized that the voltage also genesis the thickness deformation. This finding helps us to realize that a 3D elasticity-piezoelectricity study could provide more real-life physics.

Furthermore, Fig. 12 continues the achievements of the previous figure, but here several structures have been proposed, ranging from FGM-X and O, UD composite, and the pure piezoelectric beam. An interesting result observed here is that each beam has a different thickness deformation algorithm. The curves in this figure display that fabricating the smart structure on the basis of FGM and UD concepts although can create further material stiffness for the PZT matrix, the way that the beams deform is not also similar in these cases. This fact proves the significance of 3D elasticity evaluation as well. The deformations in line with the thickness show paradoxical behavior with concave and convex curves, specifying that the GNPs as a reinforcer could change the deformation pattern.

Fig. 9 revealed that the number of layers for the FGM does not fundamentally impact the maximum deflections of the different beams. Yet here via Fig. 13, where various thickness amounts are considered for GNPs, it is vivid that the GNPs' number of layers is very effectual for the thickness deformations and the displacements along with the thickness have a dissimilar path, authenticating the result attained earlier for the effect of GNPs on the orientation of deformations. An increase in the number of layers for GNPs enlarges the values of the deflections which means the stiffness of the nanocomposite decreased. This is clear from the results belonging to the GNPs with a thickness of 68nm compared to that of 6.8nm. According to Eq. (34), just after increasing the value of GNPs' thickness, the value of elasticity modulus diminishes. Consequently, the deflections look bigger. From an engineering point of view, when the GNPs are thinner, their strength is further. That is why a one-layerred GNPs (graphene sheet) could be the strongest material. As a physical supposition, this behavior could relate the homogenization rate between matrix and the filler in the nanocomposite. The thinner and smaller reinforcers could cause better homogeneity and thus the more stiffness due to the homogenized composite. However, such a practical reason should be detected in the experiments.

Examining the volume fraction of GNPs should not be restricted to the previous figures and it can be fascinating if one prepares the

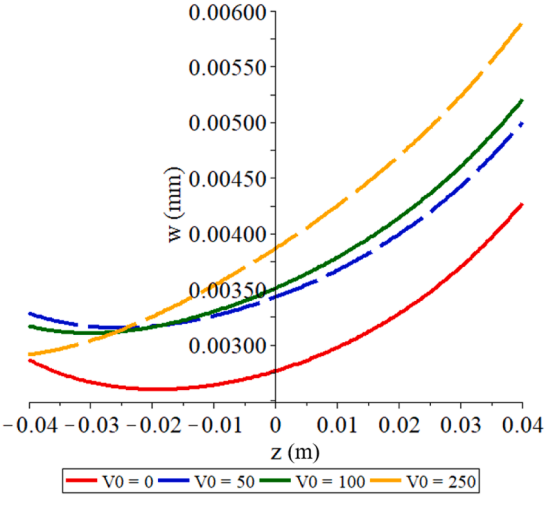

Fig. 11. Thickness deformation vs. electric voltage (FG-X).

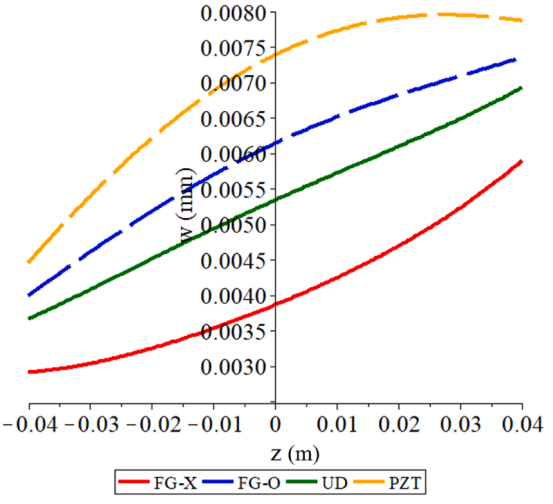

Fig. 12. Thickness deformation vs. different mixtures ($V_0 = 250$ V).

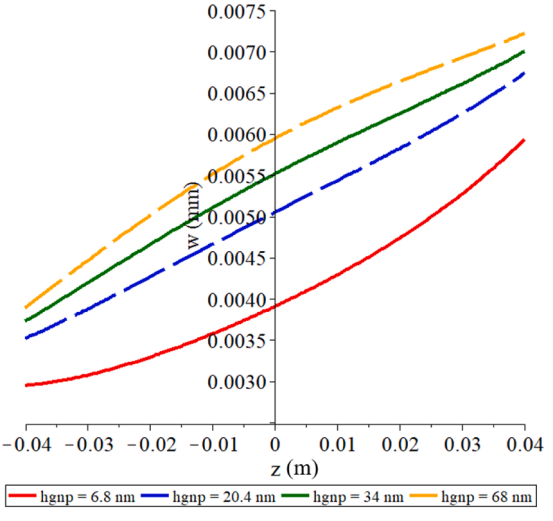

Fig. 13. Thickness deformation vs. graphene nanoplatelets thickness ($V_0 = 250$ V, FG-X).

thickness deformations utilizing different values for wt%. Thus, for this reason, Fig. 14 has been plotted. Again here it is clear that graphene volume fraction is also another effective factor that can affect the pattern of deformations in line with the thickness of the beam. The difference between results of volume fraction equivalent to zero versus those of volume fraction in the amount to one shows about twice more deflection values. It can be concluded that the presence of GNPs inside the matrix is effectual on both deflections and deformations of the 3D piezocomposite beams.

A cutting-edge 3D investigation in terms of piezoelectric composites is displayed in Fig. 15a, b, and c where the direct effect of piezoelectric constant (e) is assessed. The blue surfaces in the three figures are dedicated to the given value of e, but the other surfaces are correlated to $0.6e$, $0.8e$, and $1.2e$ respectively. The goal is to inquire into different values for the piezoelectric constant to see if it can exert influence on the elastic deformations. Interestingly, as clear, both decrease and increase in the value of the piezoelectric constant shift the forms of the surfaces. While the larger value and the lower one have resulted in entirely dissimilar results, showing that the correct value of the piezoelectric constant is worth noticing for numerical analyzes of piezoelectric structures. From the interpretation of the result and from a mathematical point of view, it can be said that because the value of piezoelectric constants is directly determinative in the relation to the electric potential (Eq. (23)), and the electric potential could then affect the function of the internal electric field along with the thickness (Eq. (14)). Afterwards, the different values of piezoelectric constants could change the form of the internal electric field's function, resulting in the alteration in the shape of the deformations through the thickness as seen in these figures. From a physical point of view, the value of piezoelectric constants stems from the piezo property of the material and such property also causes an internal electric field along with the thickness. Thus, the different forms of the internal electric field could lead to different thickness deformation patterns. One may assume that the rest of the electrical parameters that appeared in Eq. (23) should

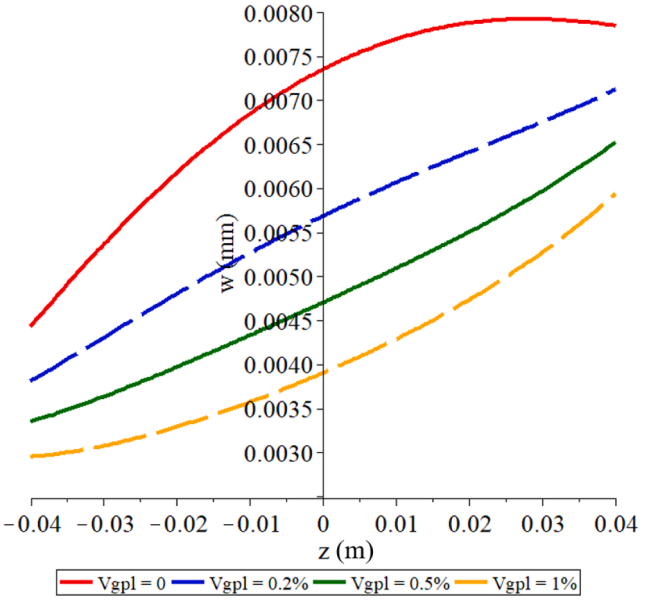

Fig. 14. Thickness deformation vs. graphene nanoplatelets' percentage ($V_0 = 250$ V, FG-X).

give such a result likewise; however, the comparison of amounts of the piezoelectric constants with those of the dielectric ones indicates that the piezoelectric constants are much more fruitful.

The discussion on the results can be ended by manifesting Fig. 16a and b. These two figures perfectly exhibit the 3D analysis by virtue of displacements through the coordinates of the length (x) and the thickness (z) of the beams simultaneously. The conflicting item in these diagrams is the absence of lateral static load for the first figure. The reason is to check out the pure effect of the electric voltage parameter on the mechanical behavior of the intelligent beams. It can be identified that while the q is excluded, there are negative/positive deflections and deformations along with the thickness, indicating that the beam twists because of the electric field. Nonetheless, the second figure denotes that the inclusion of the static load brings about different behavior and there is no rotation for the beam. It may be due to the fact that when the transverse load is imposed which is uniform and symmetrical, it causes vertical durability and the beam resists against twirling.

6. Conclusion

This paper dealt with the computational mechanical analysis of the three-dimensional elasticity-piezoelectricity of beam-like sensors/actuators made of functionally graded compositions. The motivation concerned an intelligent composite appropriate for sensing and actuating industries. The PZT-5H was supposed to be the matrix and graphene nanoplatelets have been mixed as a filler with the piezoelectric substrate in several patterns, leading to smart composites. The analysis also involved geometrical nonlinearity for the investigation of large deflections. The derived governing equations have been implemented into the generalized differential quadrature numerical technique, transferring to simpler formats for the solution possibility. To report the numerical results and underline a case study, the Newton-Raphson method has been executed. Special cases have been comprehensively discussed using reciprocal parametric studies. This study was also the first attempt to predict the mechanical behavior of piezoelectric composite structures via 3D analysis. We believe that this theoretical research adequately extends the studies on smart materials. Many results have been gained through the medium of this research summarized below,

- The beams underlying the maximum deflections are usually faced with numeric values that are unable to exemplify the thickness deformity template. Anyway, this study detected that a variety of elements could be efficacious to show by what means the thickness deforms, such as the merge of a nano-additive inside the composite, external electric voltage, FGM mixture schemes, and even the volume fraction of GNPs.
- The intelligent materials, for instance, piezoelectric ceramics, are normally brittle structures that are incapable of a desirable flexibility. To tackle this issue and build higher flexible smart sensors/actuators, graphene nanoplatelets in FGM compositions could be an advisable kind of aggregation/filler.
- The 3D electro-elastic assessment corroborated that when a smart beam undergoes an external electric field with no outer static load imposed on the structure, the beam could twist as a consequence of the electric voltage.
- The performed parametric study showed that the GNPs' volume fraction is much more determinative than the FGM's number of layers to obtain a higher efficient composite.

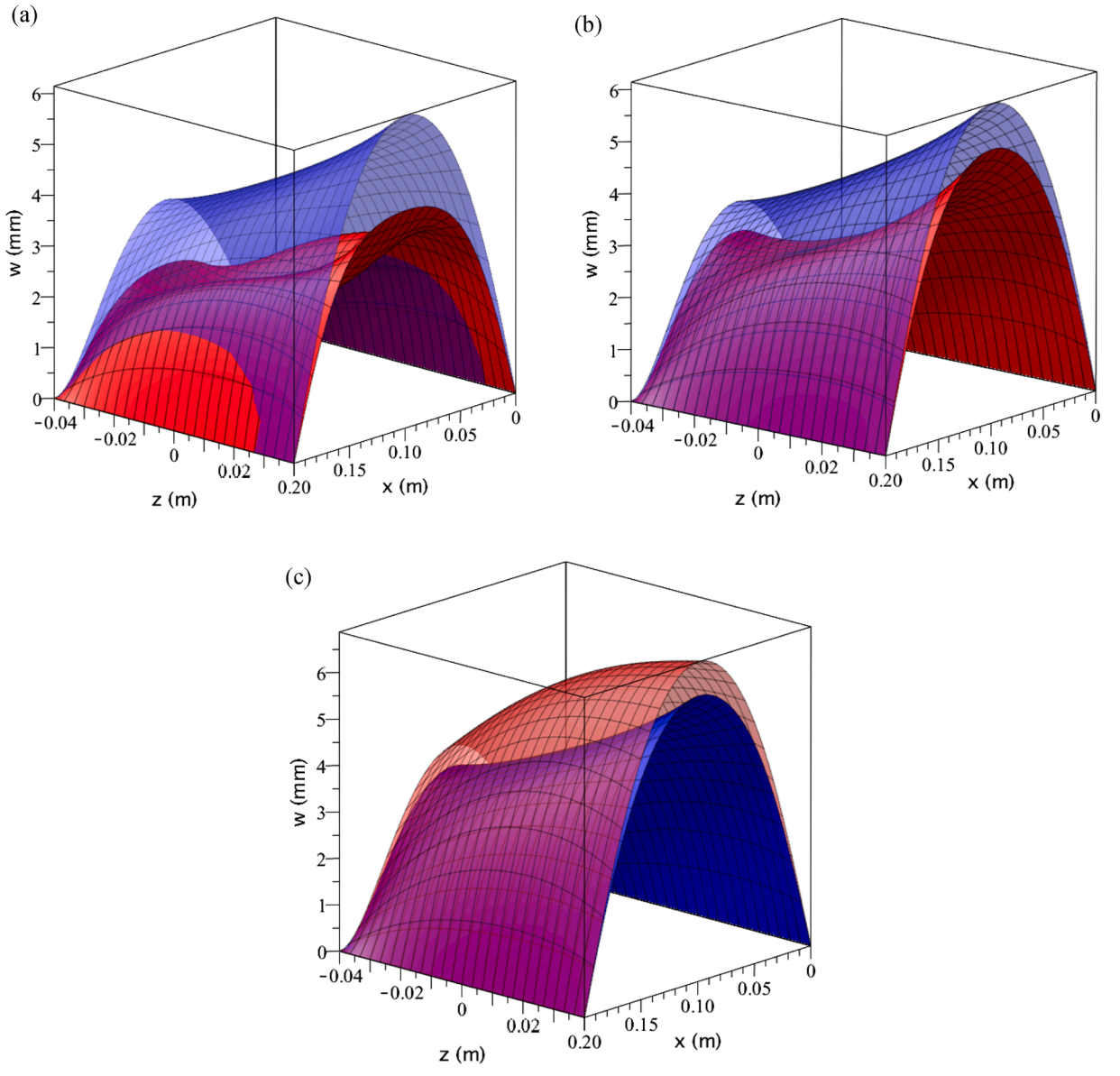

Fig. 15. a Deformations in line with length and thickness vs. piezoelectric constant ($V_0 = 250$ V, FG-X). b Deformations in line with length and thickness vs. piezoelectric constant ($V_0 = 250$ V, FG-X). c Deformations in line with length and thickness vs. piezoelectric constant ($V_0 = 250$ V, FG-X).

- The piezoelectric constant can be an outstanding parameter with regard to electro-mechanical analyzes. This factor not only gets involved in the values of deflections but also varies the thickness deformation path.
- It was acquired that the smart composite subject to an external electric field will lose its mechanical strength gradually due to an increase in the value of the electric voltage. This stiffness reduction seemed with a less steep slope in FG-X results in comparison with the rest.

CRediT authorship contribution statement

Mohammad Malikan: Writing – original draft, Supervision, Resources, Project administration, Methodology, Investigation, Funding acquisition, Formal analysis, Data curation, Conceptualization. **Shahriar Dastjerdi:** Writing – review & editing, Visualization, Validation, Software, Resources, Methodology, Investigation, Formal analysis, Data curation. **Magdalena Rucka:** Writing – review & editing, Supervision, Resources, Project administration. **Mehran Kadkhodayan:** Writing – review & editing, Investigation.

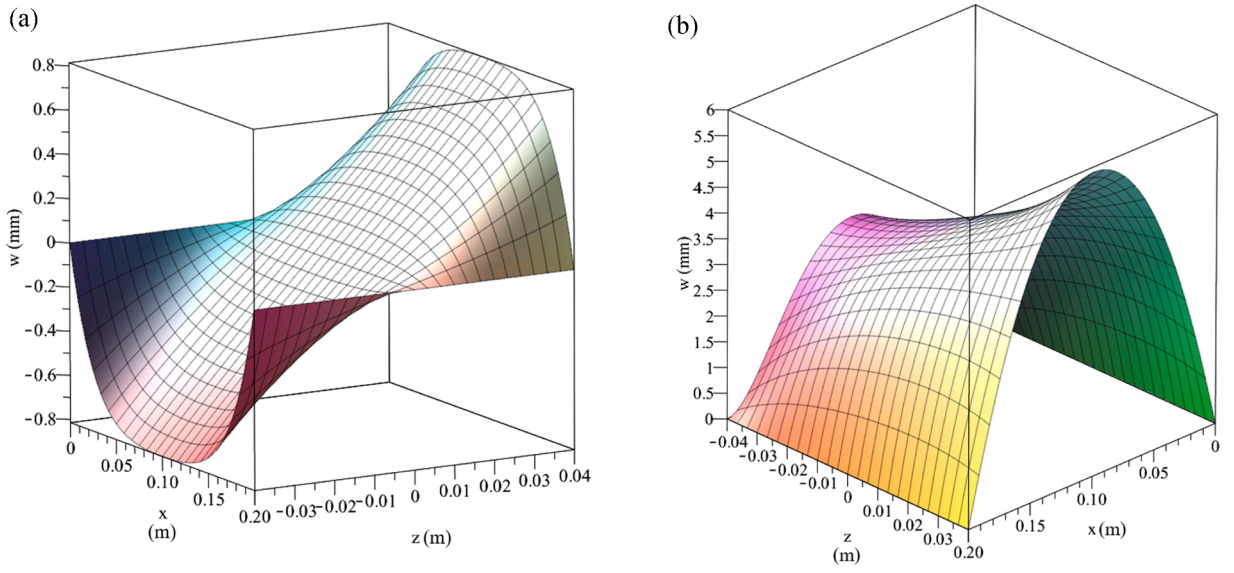

Fig. 16. a Deformations in line with length and thickness ($q = 0$, $V_0 = 250$ V, FG-X, $g_{gnp}* = 1$ %). b Deformations in line with length and thickness ($V_0 = 250$ V, FG-X, $g_{gnp}* = 1$ %).

Declaration of competing interest

There is no conflict of interest to disclose regarding this research paper.

Acknowledgments

Financial support of the study from the grant ARGENTUM TRIGGERING RESEARCH GRANTS - 'Excellence Initiative - Research University' (Project no. 9/1/2022/IDUB/I3b/Ag) which was supported by Gdańsk University of Technology, Gdańsk, Poland.

Computations were carried out using the computers of Center of Informatics Tricity Academic Supercomputer & Network

Data availability

Data is a part of future research and cannot be shared.

References

What is "Lead zirconium titanate"?". americanpiezo.com. APC International. Retrieved April 29, 2021.

ABC 2020a Piezoelectric energy harvester modeling using composite layup in ABAQUS. www.youtube.com/@finiteelementanalysismodel7282.

Affdl, J. H., & Kardos, J. (1976). The Halpin-Tsai equations: A review. *Polymer Engineering & Science, 16*, 344–352.

Akbari Alashti, R., & Khorsand, M. (2011). Three-dimensional thermo-elastic analysis of a functionally graded cylindrical shell with piezoelectric layers by differential quadrature method. *International Journal of Pressure Vessels and Piping, 88*, 167–180.

Alibeigloo, A., & Nouri, V. (2010). Static analysis of functionally graded cylindrical shell with piezoelectric layers using differential quadrature method. *Composite Structures, 92*, 1775–1785.

Alshenawy, R., Sahmani, S., Safaei, B., Elmoghazy, Y., Al-Alwan, A., & Al Nuwairan, M. (2023). Three-dimensional nonlinear stability analysis of axial-thermal-electrical loaded FG piezoelectric microshells via MKM strain gradient formulations. *Applied Mathematics and Computation, 439*, Article 127623.

Aoki, Y., Masuda, H., Tochigi, E., & Yoshida, H. (2024). Overcoming the intrinsic brittleness of high-strength Al_2O_3–$GdAlO_3$ ceramics through refined eutectic microstructure. *Nature Communications, 15*, 8700.

Arefi, M., Mohammad-Rezaei Bidgoli, E., Dimitri, R., Bacciocchi, M., & Tornabene, F. (2018). Application of sinusoidal shear deformation theory and physical neutral surface to analysis of functionally graded piezoelectric plate. *Composites Part B: Engineering, 151*, 35–50.

Argatov, II., & Sabina, FJ. (2022). Recovery of information on the depth-dependent profile of elastic FGMs from indentation experiments. *International Journal of Engineering Science, 176*, Article 103659.

Arnau, A., & Soares, D. (2009). Fundamentals of Piezoelectricity. In A. A. Vives (Ed.), *Piezoelectric transducers and applications*. Berlin, Heidelberg: Springer.

Ashoori, A. R., & Sadough Vanini, S. A. (2017). Nonlinear bending, postbuckling and snap-through of circular size-dependent functionally graded piezoelectric plates. *Thin-Walled Structures, 111*, 19–28.

Atai, A. A., & Lak, D. (2016). Analytic investigation of effect of electric field on elasto-plastic response of a functionally graded piezoelectric hollow sphere. *Journal of Mechanical Science and Technology, 30*, 113–119.

Attar, F., Khordad, R., Zarifi, A., & Modabberasl, A. (2021). Application of nonlocal modified couple stress to study of functionally graded piezoelectric plates. *Physica B: Condensed Matter, 600*, Article 412623.

Barretta, R., Luciano, R., de Sciarra, F. M., & Vaccaro, M. S. (2024). Modelling issues and advances in nonlocal beams mechanics. *International Journal of Engineering Science, 198*, Article 104042.

Bell, A. J., & Deubzer, O. (2018). Lead-free piezoelectrics—The environmental and regulatory issues. *MRS Bulletin, 43*, 581–587.

Cady, W. G. (1964). *Piezoelectricity: An introduction to the theory and applications of electromechanical phenomena in crystals* (2nd edn.,, *II*. New York: Dover Publication Inc.

Chen, W. Q., Bian, Z. G., Lv, C. F., & Ding, H. J. (2004). 3D free vibration analysis of a functionally graded piezoelectric hollow cylinder filled with compressible fluid. *International Journal of Solids and Structures, 41*, 947–964.
Chróścielewski, J., Schmidt, R., & Eremeyev, V. A. (2019). Nonlinear finite element modeling of vibration control of plane rod-type structural members with integrated piezoelectric patches. *Continuum Mechanics and Thermodynamics, 31*, 147–188.
Curie, P., & Curie, J. (1880). Développement, par pression, de l'électricité polaire dans les cristaux hémièdres à faces inclines. *Comptes Rendus, 91*, 294–295.
Dastjerdi, S., Alibakhshi, A., Akgöz, B., & Civalek, Ö. (2023b). On a comprehensive analysis for mechanical problems of spherical structures. *International Journal of Engineering Science, 183*, Article 103796.
Dastjerdi, Sh., & Akgöz, B. (2018b). New static and dynamic analyses of macro and nano FGM plates using exact three-dimensional elasticity in thermal environment. *Composite Structures, 192*, 626–641.
Dastjerdi, Sh., & Akgöz, B. (2018a). New static and dynamic analyses of macro and nano FGM plates using exact three-dimensional elasticity in thermal environment. *Composite Structures, 192*, 626–641.
Dastjerdi, Sh., Beni, Y. T, & Malikan, M. (2022). A comprehensive study on nonlinear hygro-thermo-mechanical analysis of thick functionally graded porous rotating disk based on two quasi-three-dimensional theories. *Mechanics Based Design of Structures and Machines, 50*, 3596–3625.
Dastjerdi, Sh., Civalek, Ö., Malikan, M., & Akgöz, B. (2023a). On analysis of nanocomposite conical structures. *International Journal of Engineering Science, 191*, Article 103918.
Dastjerdi, Sh., & Jabbarzadeh, M. (2016). Nonlinear bending analysis of bilayer orthotropic graphene sheets resting on Winkler–Pasternak elastic foundation based on non-local continuum mechanics. *Composites Part B: Engineering, 87*, 161–175.
Dastjerdi, Sh., & Jabbarzadeh, M. (2017). Non-linear bending analysis of multi-layer orthotropic annular/circular graphene sheets embedded in elastic matrix in thermal environment based on non-local elasticity theory. *Applied Mathematical Modelling, 41*, 83–101.
Dastjerdi, Sh., Jabbarzadeh, M., & Aliabadi, Sh. (2016). Nonlinear static analysis of single layer annular/circular graphene sheets embedded in Winkler–Pasternak elastic matrix based on non-local theory of Eringen. *Ain Shams Engineering Journal, 7*, 873–884.
Dastjerdi, Sh., Malikan, M., Eremeyev, V. A., Akgöz, B., & Civalek, Ö. (2021). On the generalized model of shell structures with functional cross-sections. *Composite Structures, 272*, Article 114192.
Deforming brittle, materials. (2023). *Nature Materials, 22*, 1161.
Du, Sh., Zhou, J., & Li, F. (2024). Dynamic deformation monitoring of cantilever beams using piezoelectric sensors: Theory and experiment. *Measurement, 227*, Article 114305.
Ebrahimi, F., & Dabbagh, A. (2019). Vibration analysis of multi-scale hybrid nanocomposite plates based on a Halpin-Tsai homogenization model. *Composites Part B: Engineering, 173*, Article 106955.
Eyvazian, A., Shahsavari, D., & Karami, B. (2020). On the dynamic of graphene reinforced nanocomposite cylindrical shells subjected to a moving harmonic load. *International Journal of Engineering Science, 154*, Article 103339.
Fan, Y., Ghayesh, M. H., Lu, T.-F., & Amabili, M. (2022). Design, development, and theoretical and experimental tests of a nonlinear energy harvester via piezoelectric arrays and motion limiters. *International Journal of Non-Linear Mechanics, 142*, Article 103974.
Farokhi, H., & Ghayesh, M. H. (2018). Nonlinear mechanical behaviour of microshells. *International Journal of Engineering Science, 127*, 127–144.
Farokhi, H., Ghayesh, M. H., & Gholipour, A. (2017). Dynamics of functionally graded micro-cantilevers. *International Journal of Engineering Science, 115*, 117–130.
Gautschi, G. (2002). *Force strain pressure acceleration and acoustic emission sensors materials and amplifiers, piezoelectric sensorics, XIII* p. 264). Berlin, Heidelberg: Springer.
Gerstner, E. Nobel Prize 2010: Andre Geim & Konstantin Novoselov. Nature Physics 6 (2010) 836. 10.1038/nphys1836.
Ghayesh, M. H. (2011). On the natural frequencies, complex mode functions, and critical speeds of axially traveling laminated beams: parametric study. *Acta Mechanica Solida Sinica, 24*, 373–382.
Golmakani, M. E., Malikan, M., Pour, S. G., & Eremeyev, V. A. (2023). Bending analysis of functionally graded nanoplates based on a higher-order shear deformation theory using dynamic relaxation method. *Continuum Mechanics and Thermodynamics, 35*, 1103–1122.
Hassanzadeh-Aghdam, M. (2021). Evaluating the effective creep properties of graphene-reinforced polymer nanocomposites by a homogenization approach. *Composites Science and Technology, 209*, Article 108791.
He, D., Li, W., Vaziri, V., & Aphale, S. S. (2024). Thermo-electro-mechanical vibration analysis for piezoelectric plates under two-parameter elastic foundation with general boundary conditions. *International Journal of Engineering Science, 201*, Article 104057.
Hosseini-Hashemi, Sh., Azimzadeh-Monfared, M., & Rokni Damavandi Taher, H. (2010). A 3-D Ritz solution for free vibration of circular/annular functionally graded plates integrated with piezoelectric layers. *International Journal of Engineering Science, 48*, 1971–1984.
Javanbakht, M., Daneshmehr, A. R., Shakeri, M., & Nateghi, A. (2012). The dynamic analysis of the functionally graded piezoelectric (FGP) shell panel based on three-dimensional elasticity theory. *Applied Mathematical Modelling, 36*, 5320–5333.
Jena, S. K., Chakraverty, S., & Malikan, M. (2021b). Application of shifted Chebyshev polynomial-based Rayleigh–Ritz method and Navier's technique for vibration analysis of a functionally graded porous beam embedded in Kerr foundation. *Engineering with Computers, 37*, 3569–3589.
Jena, S. K., Chakraverty, S., & Malikan, M. (2021a). Implementation of Haar wavelet, higher order Haar wavelet, and differential quadrature methods on buckling response of strain gradient nonlocal beam embedded in an elastic medium. *Engineering with Computers, 37*, 1251–1264.
Jodaei, A., Jalal, M., & Yas, M. H. (2013). Three-dimensional free vibration analysis of functionally graded piezoelectric annular plates via SSDQM and comparative modeling by ANN. *Mathematical and Computer Modelling, 57*, 1408–1425.
Kaplunov, J., Erbaş, B., & Ege, N. (2022). Asymptotic derivation of 2D dynamic equations of motion for transversely inhomogeneous elastic plates. *International Journal of Engineering Science, 178*, Article 103723.
Karami, B., & Ghayesh, M. H. (2023). Vibration characteristics of sandwich microshells with porous functionally graded face sheets. *International Journal of Engineering Science, 189*, Article 103884.
Karami, B., & Ghayesh, M. H. (2024b). Dynamics of graphene origami-enabled auxetic metamaterial beams via various shear deformation theories. *International Journal of Engineering Science, 203*, Article 104123.
Karami, B., & Ghayesh, M. H. (2024a). Moving load excited dynamics of multi-layered imperfect microplates based on various micromechanical models. *International Journal of Engineering Science, 197*, Article 104017.
Karami, B., Ghayesh, M. H., & Fantuzzi, N. (2024). Quasi-3D free and forced vibrations of poroelastic microplates in the framework of modified couple stress theory. *Composite Structures, 330*, Article 117840.
Karami, B., & Shahsavari, D. (2019). Nonlocal strain gradient model for thermal stability of FG nanoplates integrated with piezoelectric layers. *Smart Structures and Systems, 23*, 215–225.
Ke, L.-L., Liu, Ch., & Wang, Y.-Sh. (2015). Free vibration of nonlocal piezoelectric nanoplates under various boundary conditions. *Physica E: Low-dimensional Systems and Nanostructures, 66*, 93–106.
Kędra, R., & Rucka, M. (2017). Modelling of mechanical behaviour of high-frequency piezoelectric actuators using Bouc-Wen model. *Metrology and Measurement Systems, 24*, 413–424.
Komijani, M., Reddy, J. N., & Eslami, M. R. (2014). Nonlinear analysis of microstructure-dependent functionally graded piezoelectric material actuators. *Journal of the Mechanics and Physics of Solids, 63*, 214–227.
Kulikov, G. M., & Plotnikova, S. V. (2013). A new approach to three-dimensional exact solutions for functionally graded piezoelectric laminated plates. *Composite Structures, 106*, 33–46.
Le, K. C. (2017). An asmptotically exact theory of functionally graded piezoelectric shells. *International Journal of Engineering Science, 112*, 42–62.
Li, Ch., Han, Q., Wang, Zh., & Wu, X. (2020). Analysis of wave propagation in functionally graded piezoelectric composite plates reinforced with graphene platelets. *Applied Mathematical Modelling, 81*, 487–505.
Li, X. Y., Wang, Z. K., & Huang, S. H. (2004). Love waves in functionally graded piezoelectric materials. *International Journal of Solids and Structures, 41*, 7309–7328.

Li, X. Y., Wu, J., Ding, H. J., & Chen, W. Q. (2011). 3D analytical solution for a functionally graded transversely isotropic piezoelectric circular plate under tension and bending. *International Journal of Engineering Science, 49*, 664–676.
Liang, X., Deng, Y., Cao, Z., Jiang, X., Wang, T., Ruan, Y., & Zha, X. (2019). Three-dimensional dynamics of functionally graded piezoelectric cylindrical panels by a semi-analytical approach. *Composite Structures, 226*, Article 111176.
Lin, Ch.-H., & Muliana, A. (2015). Nonlinear electro-mechanical responses of functionally graded piezoelectric beams. *Composites Part B: Engineering, 72*, 53–64.
Lu, J., Yu, C., Xu, W., & Chiu, C. (2021). Characteristic orthogonal polynomials-Ritz method for vibration behavior of functionally graded piezoelectric plates using FSDT. *Computers & Mathematics with Applications, 98*, 157–168.
Malekzadeh, P., Setoodeh, A. R., & Shojaee, M. (2018). Vibration of FG-GPLs eccentric annular plates embedded in piezoelectric layers using a transformed differential quadrature method. *Computer Methods in Applied Mechanics and Engineering, 340*, 451–479.
Malikan, M. (2017). Electro-mechanical shear buckling of piezoelectric nanoplate using modified couple stress theory based on simplified first order shear deformation theory. *Applied Mathematical Modelling, 48*, 196–207.
Malikan, M. (2018). Temperature influences on shear stability of a nanosize plate with piezoelectricity effect. *Multidiscipline Modeling in Materials and Structures, 14*, 125–142.
Malikan, M. (2019). Electro-thermal buckling of elastically supported double-layered piezoelectric nanoplates affected by an external electric voltage. *Multidiscipline Modeling in Materials and Structures, 15*, 50–78.
Malikan, M. (2024). On mechanics of piezocomposite shell structures. *International Journal of Engineering Science, 198*, Article 104056.
Malikan, M., Dastjerdi, Sh., Eremeyev, V. A., & Sedighi, H. M. (2023). On a 3D material modelling of smart nanocomposite structures. *International Journal of Engineering Science, 193*, Article 103966.
Malikan, M., & Eremeyev, V. A. (2020b). A new hyperbolic-polynomial higher-order elasticity theory for mechanics of thick FGM beams with imperfection in the material composition. *Composite Structures, 249*, Article 112486.
Malikan, M., & Eremeyev, V. A. (2020a). On the dynamics of a visco–piezo–flexoelectric nanobeam. *Symmetry, 12*, 643.
Malikan, M., & Eremeyev, V. A. (2023). On time-dependent nonlinear dynamic response of micro-elastic solids. *International Journal of Engineering Science, 182*, Article 103793.
Malikan, M., Jabbarzadeh, M., & Dastjerdi, Sh. (2017). Non-linear static stability of bi-layer carbon nanosheets resting on an elastic matrix under various types of in-plane shearing loads in thermo-elasticity using nonlocal continuum. *Microsystem Technologies, 23*, 2973–2991.
Malikan, M., & Sadraee Far, M. N. (2018). Differential quadrature method for dynamic buckling of graphene sheet coupled by a viscoelastic medium using neperian frequency based on nonlocal elasticity theory. *Journal of Applied and Computational Mechanics, 4*, 147–160.
Malikan, M., Wiczenbach, T., & Eremeyev, V. A. (2022). Thermal buckling of functionally graded piezomagnetic micro- and nanobeams presenting the flexomagnetic effect. *Continuum Mechanics and Thermodynamics, 34*, 1051–1066.
Manbachi, A., & Cobbold, R. S. C. (2011). Development and application of piezoelectric materials for ultrasound generation and detection. *Ultrasound (Leeds, England), 19*, 187–196.
Markov, A., Markov, M., Levin, V., & Jarillo, G. R (2023). Electromagnetic field excitation during the scattering of an acoustic wave on an inhomogeneity in a poroelastic medium. *International Journal of Engineering Science, 182*, Article 103784.
Mirfatah, S. M., Shahmohammadi, M. A., Salehipour, H., & Civalek, Ö. (2024). On nonlinear buckling of microshells. *International Journal of Engineering Science, 199*, Article 104077.
Moghadasi, K., Ghayesh, M. H., Hu, E., & Li, J. (2024). Nonlinear biomechanics of diseased carotid arteries. *International Journal of Engineering Science, 199*, Article 104070.
Moreno-Mateos, M. A., Mehnert, M., & Steinmann, P. (2024). Electro-mechanical actuation modulates fracture performance of soft dielectric elastomers. *International Journal of Engineering Science, 195*, Article 104008.
Nguyen, L. B., Thai, Ch. H., Zenkour, A. M., & Nguyen-Xuan, H. (2019). An isogeometric Bézier finite element method for vibration analysis of functionally graded piezoelectric material porous plates. *International Journal of Mechanical Sciences, 157-158*, 165–183.
Nguyen, N. V., & Lee, J. (2021). On the static and dynamic responses of smart piezoelectric functionally graded graphene platelet-reinforced microplates. *International Journal of Mechanical Sciences, 197*, Article 106310.
Ninh, D. G., Vang, T. V., Ha, N. H., Long, N. T., Nguyen, C. T., & Dao, D. V. (2022). Effect of cracks on dynamical responses of double-variable-edge plates made of graphene nanoplatelets-reinforced porous matrix and sur-bonded by piezoelectric layers subjected to thermo-mechanical loads. *European Journal of Mechanics - A/Solids, 96*, Article 104742.
Partovi Shabestari, N., Rashidian Vaziri, M. R., Bakhshandeh, M., Alidokht, I., & Alizadeh, Y. (2019). Fabrication of a simple and easy-to-make piezoelectric actuator and its use as phase shifter in digital speckle pattern interferometry. *Journal of Optics, 48*, 272–282.
Prolongo, S. G., Jiménez-Suárez, A., Moriche, R., & Ureña, A. (2014). Graphene nanoplatelets thickness and lateral size influence on the morphology and behavior of epoxy composites. *European Polymer Journal, 53*, 292–301.
Rafiee, M., He, X. Q., & Liew, K. M. (2014a). Non-linear dynamic stability of piezoelectric functionally graded carbon nanotube-reinforced composite plates with initial geometric imperfection. *International Journal of Non-Linear Mechanics, 59*, 37–51.
Rafiee, M., Liu, X. F., He, X. Q., & Kitipornchai, S. (2014b). Geometrically nonlinear free vibration of shear deformable piezoelectric carbon nanotube/fiber/polymer multiscale laminated composite plates. *Journal of Sound and Vibration, 333*, 3236–3251.
Saidi, A. R., Bahaadini, R., & Majidi-Mozafari, K. (2019). On vibration and stability analysis of porous plates reinforced by graphene platelets under aerodynamical loading. *Composites Part B: Engineering, 164*, 778–799.
Saleh, B., Jiang, J., Fathi, R., Al-hababi, T., Xu, Q., Wang, L., Song, D., & Ma, A. (2020). 30 years of functionally graded materials: An overview of manufacturing methods, applications and future challenges. *Composites Part B: Engineering, 201*, Article 108376.
Samadhiya, R., & Mukherjee, A. (2006). Functionally graded piezoceramic ultrasonic transducers. *Smart Materials and Structures, 15*, 627–631.
Shariff, M. H. B. M., & Bustamante, R. (2024). On a class of implicit constitutive relations for nonlinear elastic bodies. *International Journal of Engineering Science, 200*, Article 104089.
Shen, H.-Sh., & Yang, D.-Q. (2015). Nonlinear vibration of functionally graded fiber reinforced composite laminated beams with piezoelectric fiber reinforced composite actuators in thermal environments. *Engineering Structures, 90*, 183–192.
Shokrieh, M. M., Ghoreishi, S. M., Esmkhani, M., & Zhao, Z. (2014). Effects of graphene nanoplatelets and graphene nanosheets on fracture toughness of epoxy nanocomposites. *Fatigue & Fracture of Engineering Materials & Structures, 37*, 1116–1123.
Silva, T. M. P., Hameury, C., Ferrari, G., Balasubramanian, P., Franchini, G., & Amabili, M. (2023). Particle swarm optimization of a non-collocated MIMO PPF active vibration control of a composite sandwich plate. *Journal of Sound and Vibration, 555*, Article 117723.
Singh, A., Naskar, S., Kumari, P., & Mukhopadhyay, T. (2023). Viscoelastic free vibration analysis of in-plane functionally graded orthotropic plates integrated with piezoelectric sensors: Time-dependent 3D analytical solutions. *Mechanical Systems and Signal Processing, 184*, Article 109636.
Singh, D., Kiran, R., Chawla, K., Kumar, R., Chauhan, V. S., & Vaish, R. (2022). Determination of multi-physics effective properties, and actuation response of triply periodic minimal surface based novel photostrictive composites: A finite element analysis. *International Journal of Engineering Science, 178*, Article 103726.
Steinem, C., & Janshoff, A. (2005). Sensors | Piezoelectric resonators. In P Worsfold, A Townshend, & C Poole (Eds.), *Encyclopedia of analytical science* (Second Edition, pp. 269–276). Elsevier.
Stempin, P., Pawlak, T. P., & Sumelka, W. (2023). Formulation of non-local space-fractional plate model and validation for composite micro-plates. *International Journal of Engineering Science, 192*, 103932.
Su, Zh., Jin, G., & Ye, T. (2018). Electro-mechanical vibration characteristics of functionally graded piezoelectric plates with general boundary conditions. *International Journal of Mechanical Sciences, 138–139*, 42–53.
Tabatabaei-Nejhad, S. Z., Malekzadeh, P., & Eghtesad, M. (2020). Out-of-plane vibration of laminated FG-GPLRC curved beams with piezoelectric layers. *Thin-Walled Structures, 150*, Article 106678.

Takagi, K., Li, J.-F., Yokoyama, Sh., & Watanabe, R. (2003). Fabrication and evaluation of PZT/Pt piezoelectric composites and functionally graded actuators. *Journal of the European Ceramic Society, 23*, 1577–1583.
Tanaka, T. (1982). Piezoelectric devices in Japan. *Ferroelectrics, 40*, 167–187.
Taya, M., Almajid, A. A., Dunn, M., & Takahashi, H. (2003). Design of bimorph piezo-composite actuators with functionally graded microstructure. *Sensors and Actuators A: Physical, 107*, 248–260.
Vaccaro, M. S. (2022). On geometrically nonlinear mechanics of nanocomposite beams. *International Journal of Engineering Science, 173*, Article 103653.
Wang, B. L., & Noda, N. (2001). Design of a smart functionally graded thermopiezoelectric composite structure. *Smart Materials and Structures, 10*, 189–193.
Wang, H. M., & Xu, Z. X. (2010). Effect of material inhomogeneity on electromechanical behaviors of functionally graded piezoelectric spherical structures. *Computational Materials Science, 48*, 440–445.
Wang, Y., Ding, H., & Xu, R. (2016). Three-dimensional analytical solutions for the axisymmetric bending of functionally graded annular plates. *Applied Mathematical Modelling, 40*, 5393–5420.
Wankhade, R. L., & Bajoria, K. M. (2013). Buckling analysis of piezolaminated plates using higher order shear deformation theory. *International Journal of Composite Materials, 3*, 92–99.
Wudy, F., Stock, C., & Gores, H. J. (2009). Measurement methods | Electrochemical: Quartz microbalance. In J Garche (Ed.), *Encyclopedia of electrochemical power sources* (pp. 660–672). Elsevier.
Xia, H., & Gu, Y. (2021). Generalized finite difference method for electroelastic analysis of three-dimensional piezoelectric structures. *Applied Mathematics Letters, 117*, Article 107084.
Yamada, K., Sakamura, J., & Nakamura, K. (1998). Broadband ultrasound transducers using effectively graded piezoelectric materials. In *IEEE Ultrasonics Symposium* (pp. 1085–1089).
Yang, Y., Dai, T., & Dai, H.-L. (2023). Hygro-thermo-mechanical coupling behavior of porous FG-GNPRC annular plates considering aggregation of GNPs. *Thin-Walled Structures, 192*, Article 111145.
Yee, K., & Ghayesh, M. H. (2023). A review on the mechanics of graphene nanoplatelets reinforced structures. *International Journal of Engineering Science, 186*, Article 103831.
Yiqi, M., & Yiming, F. (2010). Nonlinear dynamic response and active vibration control for piezoelectric functionally graded plate. *Journal of Sound and Vibration, 329*, 2015–2028.
Zenkour, AM., & Aljadani, MH. (2020). Buckling analysis of actuated functionally graded piezoelectric plates via a quasi-3D refined theory. *Mechanics of Materials, 151*, Article 103632.
Zhong, Z., & Shang, E. T. (2003). Three-dimensional exact analysis of a simply supported functionally gradient piezoelectric plate. *International Journal of Solids and Structures, 40*, 5335–5352.
Zhou, K., Hu, Zh., & Hua, H. (2021b). Investigation of the nonstationary stochastic response of functionally graded piezoelectric material plates with general boundary conditions. *Applied Mathematical Modelling, 96*, 315–335.
Zhou, K., Hu, Zh., & Hua, H. (2021a). Investigation of the nonstationary stochastic response of functionally graded piezoelectric material plates with general boundary conditions. *Applied Mathematical Modelling, 96*, 315–335.